Attention is drawn to the fact that the copyright of this thesis rests with its author.

This copy of the thesis has been supplied on condition that anyone who consults it is understood to recognise that its copyright rests with its author and that no quotation from the thesis and no information derived from it may be published without the author's prior written consent.

D 12781/75
Otley, T.W.
PP112

Errata

p. 43, l. 27 equation should read $J_o = \frac{2{\cdot}3\ V_o^{3/2}}{D^2}$,

where D is the cathode - anode separation (~1 cm).

p. 44, l. 6 replace Spanenberg by Spangenberg, also in figure caption.

p. 46, l. 23 replace flourescent by fluorescent.

p. 95, l. 16 replace Spanenberg by Spangenberg.

ration (~1 cm).

lso in

POLARISATION OF THE $6^1S_0 - 6^1P_1$ AND $6^1S_0 - 6^3P_1$ LINES OF MERCURY, EXCITED BY ELECTRON IMPACT

T.W.Ottley

Department of Physics, University of Stirling

July, 1974

Abstract

The polarisation of the $6^1S_0 - 6^1P_1$ (1850 A) and the $6^1S_0 - 6^3P_1$ (2537 A) lines of mercury, excited by low energy electron impact, have been measured. In both cases, the emitted radiation was observed in a direction perpendicular to the electron beam. In the first instance, the polarisation of the 2537 A line was measured with an energy resolution of 300 meV, in an experiment where the mercury was in the form of a vapour. The results from this gave a first indication that resonances in the excitation of the line are responsible for departures of the polarisation from the theory of McConnell and Moiseiwitsch.

A crossed-beam apparatus was assembled, and the polarisation of the 1850 A line was measured, again under low resolution. Agreement with the theory in this case is reasonable, apart from in the region within a few eV of threshold, where the measured polarisation is rather lower than that predicted.

To examine more carefully the resonances observed in the 2537 A line, an electron monochromator was built, and the polarisation of the line was measured under high resolution. Data are presented with an energy resolution of 140 meV and 100 meV. A total of six features are observed, of which resonances at 4·92 and 5·50 eV are particularly well marked. The observed polarisation of the resonance at 4·92 eV appears to be in agreement with the hypothesis that a $^4P_{3/2}$ negative ion state of mercury is being formed at that energy.

Acknowledgements

Firstly, I wish to thank Dr.D.R.Denne who designed several parts of the vapour experiment, and often assisted in the later stages of the work. I also thank B.J.Benson, who built up much of the first apparatus.

Throughout the course of this work, I have been able to seek advice from all the research workers at Stirling; Dr. A.J.Duncan and Dr. M.C.Standage I thank particularly. I am extemely grateful to V.Raible for lending me workshop drawings of the electron monochromator. I acknowledge technical assistance from the Shared Technical Services of the University of Stirling.

I wish to thank Dr. S.C.McFarlane for several valuable discussions on the possibility of resonances being responsible for the observed polarisation behaviour of the 2537 A line, and Professor P.D.Burrow for allowing me to use unpublished data from his electron transmission experiments.

I am deeply indepted to Professor H.Kleinpoppen for his unfailing support and encouragement throughout the course of this research.

I acknowledge financial support from the Science Research Council and the University Grants Committee, and a studentship from the University of Stirling.

Table of Contents

Section		Page
1	Introduction	1
2	The Experiment	7
3	Theory	
3.1	Polarisation of Radiation from the Electron Impact Excitation of Atoms	9
3.2	The Atomic System	12
3.3	Application to the 6^1P_1 and 6^3P_1 Levels of Mercury	15
3.4	Simplified Expressions for Threshold Polarisation	21
4	Apparatus for the Vapour Experiment	
4.1	General	23
4.2	Electron Gun	26
4.3	Optics	27
4.4	Electronics	29
5	Results from the Vapour Experiment	
5.1	Results	31
5.2	Sources of Error and Corrections	
5.2.1	Pressure Depolarisation	31
5.2.2	Instrumental Polarisation	34
5.2.3	Divergence of the Electron Beam	36
5.2.4	Solid Angle of Photon Detection	36
5.2.5	Possibility of other Lines being detected	37
5.2.6	Magnetic Field Depolarisation	37
6	Apparatus for the Measurement of the 1850 A Line	
6.1	The Crossed - beam Apparatus	39
6.2	The Mercury Beam	39
6.3	The Two - stage Electron Gun	41
6.4	Optics	46
6.5	Electronics	51

7 Results from the 1850 A Line Measurement

7.1 Results 52

7.2 Errors and Corrections

7.2.1 Pressure Depolarisation 56

7.2.2 Instrumental Polarisation 56

7.2.3 Other Sources of Error 59

8 High Resolution Study of the 2537 A Line

8.1 General 60

8.2 Monochromator 60

8.3 Optics 64

8.4 Electronics 64

9 Results from the High Resolution Experiment

9.1 Results 66

9.2 Sources of Error and Corrections

9.2.1 Pressure Depolarisation 70

9.2.2 Instrumental Polarisation 71

9.2.3 Divergence of the Electron Beam 74

9.2.4 Other Sources of Error 75

10 Discussion of the Results

10.1 The 1850 A Line 77

10.2 The 2537 A Line 79

10.3 Calibration of the Energy Scale

10.3.1 The 1850 A Line 83

10.3.2 The 2537 A Line 83

10.4 Discussion of the Resonances in the 2537 A Line

10.4.1 Positions of the Resonances 84

10.4.2 Identification of the Resonances 87

Appendix 1 90

Correction to Polarisation Measurements due to the Finite Convergence Angle of the Electron Beam

Appendix 2 92

Correction to Polarisation Measurements due to the Finite Solid Angle of Photon Detection

References 94

TO BARBARA

1. Introduction

When atoms of a gas or vapour are excited from the ground state to an excited state by collisions with an incident beam of electrons, the radiation emitted in subsequent electric dipole transitions, is in general, partially polarised. The relevant measurable quantities are $I_{//}$ and $I_{\perp}$, the intensities of the radiation having electric vectors parallel, and perpendicular, respectively to the electron beam direction. The fractional polarisation, P, is defined by the relation,

$$P = \frac{I_{//} - I_{\perp}}{I_{//} + I_{\perp}} .$$

The polarisation usually has a strong dependence on the energy of the exciting electrons, and, in addition, may be expected to be a function of the target gas pressure and other experimental conditions. In particular, many of the early measurements were made with a poor energy resolution, which smeared out any resonant structure.

The earliest measurements of the polarisation of line radiation excited by electron impact were made in the 1920s. In 1925, Kossel and Gerthsen[1] found that the unresolved sodium D lines showed no polarisation within the limits of their experimental uncertainty. This result was confirmed in the following year by Ellett, Foote and Mohler[2], who also tried mercury for the first time, and determined a polarisation of - 0·3 for the 2537 A line at an incident electron energy of between 6 and 7 eV. Also in 1926, Skinner[3] measured the polarisation of some 21 mercury lines, and Eldridge and Olsen[4] examined 30 mercury lines.

These early results however were mostly qualitative, being made at a fixed electron energy, and employing photographic techniques for the estimation of the relative intensities of $I_{//}$ and $I_{\perp}$. Some

comparisons with a simple theory were made with varying success. The effects of radiation trapping were not fully understood.

Quarder[5], in 1927, was able to show that there was a definite dependence of the polarisation of some of the mercury lines on the incident electron energy. His energy range extended from 16 eV to 2200 eV. This work was closely followed by the now famous paper of Skinner and Appleyard[6], where 28 mercury lines were examined, and the polarisation was measured as a function of energy. Except in the cases where the light was apparently unpolarised, these lines all showed a basically similar feature: the polarisation just above threshold was zero, or nearly so, and then as the electron energy was increased, the polarisation rose sharply to a maximum value, and then declined gradually. In some cases the polarisation changed sign at an electron energy of about 80 eV. Table 1:1 lists the lines of mercury for which polarisation measurements have been made.

Following the publication of papers by Oppenheimer[7,8] in 1927 and 1928, and by Penney[9] in 1932,on the theory of the polarisation of line radiation, it became clear that there was a serious discrepancy between the observations of Skinner and Appleyard near threshold, and the theoretical threshold polarisation values. This discrepancy existed for many years, but papers by Federov and Mezentsev[10], and Heideman, Smit and Smit[11], and the present work have shown that the energy resolution used by Skinner and Appleyard was not sufficient to observe detailed structure in the polarisation near threshold.

Although the Oppenheimer - Penney theory, as it became known, allowed for the fine- and hyperfine- structure of the atomic levels, there were several cases (such as the Lyman α line of hydrogen) where the line width was comparable to either the fine- or hyperfine-

Table 1:1 Measurements of the Polarisation of Mercury Lines Excited by Electron Impact

Wavelength	Transition	Refs.	Wavelength	Transition	Refs.
5791	$6^1P_1 - 6^1D_2$	5,6,11	3021	$6^3P_2 - 7^3D_3$	4,5,6
5770	$6^1P_1 - 6^3D_2$	5,6,10, 11	2967	$6^3P_0 - 6^3D_1$	4,5,6
5461	$6^3P_2 - 7^3S_1$	5,6,10	2925	$6^3P_2 - 9^3S_1$	4,5,6
4916	$6^1P_1 - 8^1S_0$	5,10	2894	$6^3P_1 - 8^3S_1$	4,5,6
4358	$6^3P_1 - 7^3S_1$	4,5,6, 10,11	2848	$6^3P_1 - 8^1S_0$	4
4348	$6^1P_1 - 7^1D_2$	4,5,6, 10,11	2804	$6^3P_2 - 8^3D_2$	4
4108	$6^1P_1 - 9^1S_0$	4,5,6	2803	$6^3P_2 - 8^3D_3$	5,6
4078	$6^3P_1 - 7^1S_0$	4,5,6, 10	2760	$6^3P_2 - 10^3S_1$	4
4047	$6^3P_0 - 7^3S_1$	4,5,6, 10	2753	$6^3P_0 - 8^3S_1$	4
3906	$6^1P_1 - 8^1D_2$	4,5,6	2701	$6^3P_2 - 8^1D_2$	4
3802	$6^1P_1 - 10^1S_0$	5	2700	$6^3P_2 - 8^3D_2$	4
3704	$6^1P_1 - 9^1D_2$	5,6	2699	$6^3P_2 - 8^3D_3$	4
3663	$6^3P_2 - 6^1D_2$	4,5,6	2655	$6^3P_1 - 7^1D_2$	4,5,6
3655	$6^3P_2 - 6^3D_2$	4,5,6	2654	$6^3P_1 - 7^3D_1$	4,6
3650	$6^3P_2 - 6^3D_3$	4,5,6	2652	$6^3P_1 - 7^3D_2$	4,5,6
3593	$6^1P_1 - 10^1D_2$	5	2537	$6^1S_0 - 6^3P_1$	2,5,6, 25
3341	$6^3P_2 - 8^3S_1$	4,5,6	2535	$6^3P_0 - 7^3D_1$	6
3132	$6^3P_1 - 6^1D_2$	4,5,6	2484	$6^3P_1 - 8^1D_2$	5
3126	$6^3P_1 - 6^3D_2$	4,5,6	2482	$6^3P_1 - 8^3D_2$	5
3027	$6^3P_2 - 7^1D_2$	4,5,6	2399	$6^3P_1 - 9^3D_2$	5
3026	$6^3P_2 - 7^3D_1$	4	1850	$6^1S_0 - 6^1P_1$	26
3023	$6^3P_2 - 7^3D_2$	4,5,6			

structure splitting, when the Oppenheimer - Penney theory failed to give unambiguous results. In 1958, Percival and Seaton[12] completely reviewed the polarisation theory, and showed that it was possible to treat such intermediate cases by calculating the probability of a polarised photon being emitted by the complete system of electron and atom.

Since 1958, there have been many experiments performed on the polarisation of line radiation, from a variety of different atoms and ions, but particularly helium, mercury and the alkali atoms. Helium is of particular interest here, because it is, like mercury, a two - electron system; but, unlike mercury, there is no breakdown of LS coupling. Early experiments had suggested that the polarisation was nearly zero at threshold for a number of lines where the theoretical polarisation was actually large. McFarland[13], in 1964, was able to show that if the electron energy was reduced to a value sufficiently close to threshold, then the polarisation started rising again. This has been confirmed by other experiments, of which the most important are those of Heddle and Keesing[14], and Heddle, Keesing and Watkins[15]. This last work demonstrates very clearly how rapidly the polarisation may vary in a narrow energy range just above threshold.

Similarly, in mercury, Federov and Mezentsev[10], and Heideman, Smit and Smit[11] showed that sharp changes in polarisation could exist near the threshold of a line. Often, the use of some form of electron monochromator, to reduce the energy spread normally present in an electron beam, has resulted in a measurement which has been of more value in testing the theory.

The polarisation does not always vary rapidly in the immediate vicinity of threshold. Lithium and sodium exhibit smooth variations,

as Hafner, Kleinpoppen and Kruger[16] have demonstrated. Enemark[17] found substantially similar behaviour for the sodium D lines. These results are in good agreement with theory. The results of Ehlers and Gallagher[18] for the $^1P_1 - {}^1S_0$ resonance line of calcium indicate that the predicted threshold polarisation of + 1·0 is correct, and show also that there is an initial drop in polarisation extending over a volt.

In hydrogen, the polarisation of the H_α line has been measured by Kleinpoppen and Kraiss[19], and that of the Lyman α line by Ott, Kauppila and Fite[20]. In both cases, as the electron energy is reduced towards threshold, the polarisation first rises to a maximum, and then falls abruptly to a low value near threshold.

Many fluctuations in measured polarisation functions are now known to be caused by resonances where a negative ion state is formed. The reactions possible are:

$$(a) \qquad e + A \longrightarrow A^* + e$$

$$(b) \qquad e + A \longrightarrow A^{-*} \longrightarrow A^* + e$$

(a) is the 'normal' excitation process, A^* being an excited state of the atom A; (b) is where an excited negative ion state with a typical lifetime of 10^{-14}s is formed as an intermediary. The formation of this negative ion state has the effect of increasing the overall cross - section of the A^* state, and it is in the vicinity of such resonances that the polarisation may be expected to change rapidly. The polarisation of resonances occuring near threshold has been discussed by Baranger and Gerjuoy[21]. Crandall, Taylor and Dunn[22] have found a series of resonances in the excitation

of the Ba^+ ion; in the polarisation they show up as a series of oscillations superimposed on a smooth variation with energy.

Reviews of the polarisation of atomic line radiation have been presented by Heddle and Keesing[23], Kleinpoppen[24], and by Fano and Macek[27] who have described a new formulation of the theory, based on the alignment and orientation of the radiating atoms.

2. The Experiment

In 1968, McConnell and Moiseiwitsch[28] presented careful calculations made on the polarisation of the $6^1S_0 - 6^1P_1$ (1850 A) and $6^1S_0 - 6^3P_1$ (2537 A) lines of mercury, excited by electron impact. They employed the Ochkur[29] approximation in evaluating the exchange integrals, and took into account the spin - orbit interaction which occurs in mercury. The effects of the different isotopes which constitute 'natural' mercury were also brought into the calculation. Only the polarisation of the 2537 A line had been previously measured (by Skinner and Appleyard[6]), but the measurements were not extensive enough to provide any real test of the theory.

The object of the experiment was then, in the first instance to measure the polarisation of the 1850 A and 2537 A lines as accurately as possible, using fairly straightforward modern techniques, and to compare the results with the calculations of McConnell and Moiseiwitsch. Subsequently, an electron monochromator was to be built, and used to examine any unresolved features found in the first part of the work. Such features were found in the 2537 A line.

Thus the project fell naturally into three main parts:

1) Low resolution measurement of the polarisation of the 2537 A line.
2) Low resolution measurement of the polarisation of the 1850 A line.
3) High energy-resolution study of the 2537 A line.

In each case the polarisation of the radiation emitted at an angle of 90° to the electron beam direction was measured as a function of the incident electron energy.

For the first part, an existing glass apparatus was used, in

which the mercury target was in the form of a vapour. A Pierce[30] design electron gun was used. For the second and third parts, a new crossed - beam apparatus was constructed, in which the mercury target was then in the form of an atomic beam. For the 1850 A line measurements a two - stage electron gun was built, which provided rather higher currents than had been obtainable with the Pierce gun. A high current was necessary to offset the inefficiency of the optical system at this wavelength.

For the third part, a 127° cylindrical - geometry electron monochromator was constructed. With typical currents of 2×10^{-7} A, it was still possible to measure the polarisation of the 2537 A line, although the 1850 A line would not have been possible under high resolution, due to the comparatively lower sensitivity of the detection system at that wavelength. Resonances were clearly observed using the energy-selected electrons, and the polarisation of the resonances was measured.

In each part of the experiment, great care had to be taken to ensure that instrumental effects such as pressure depolarisation were avoided, and to correct for the effects of instrumental polarisation, electron beam divergence, and the finite solid angle of photon detection.

Comparison of the results with the theoretical predictions of McConnell and Moiseiwitsch[28] have been made wherever possible, and, in the case of the resonances, comparison has been made with the calculations of Baranger and Gerjuoy[21], leading to a possible identification of the negative ion states being formed.

3. Theory

3.1 Polarisation of Radiation from the Electron Impact Excitation of Atoms.

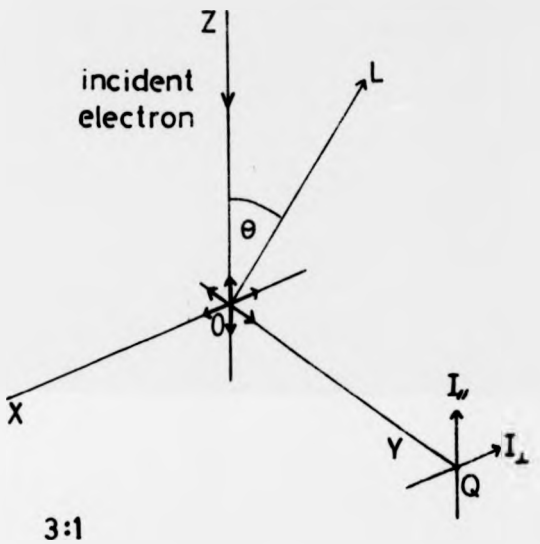

3:1

Refering to fig. 3:1, an atom, initially in the ground state is at the point O, and is excited by an incident electron travelling along ZO. The atom then decays spontaneously, emitting a photon. The radiating atom may be characterised by three orthogonal dipoles which lie along OX, OY, and OZ. At a point Q, which lies along the Y axis, the polarisation is defined to be:

$$P = \frac{I_{//} - I_{\perp}}{I_{//} + I_{\perp}} \quad , \qquad (3 - 1)$$

where the subscripts refer to the direction of the E - vector of the radiation compared to the incident electron direction, i.e. either parallel or perpendicular.

Let the intensity of radiation coming from the dipole which lies

along OZ be I_z as measured in the XY plane. This is therefore the peak intensity for the dipole. Thus the polarisation may be written

$$P = \frac{I_z - I_x}{I_z + I_x} \quad . \qquad (3 - 2)$$

The atom is assumed to be symmetric about OZ and hence

$$I_x = I_y \quad . \qquad (3 - 3)$$

Now consider a single dipole (fig. 3:2) .

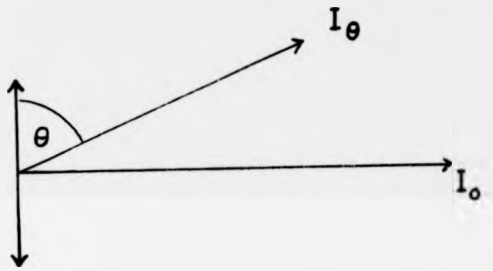

3:2

From the usual dipole characteristics,

$$I(\theta) = I_o \sin^2\theta$$

The average intensity per steradian of radiation coming from the dipole is given by,

$$\bar{I} = \frac{2\pi \int_0^\pi I_o \sin^2\theta \sin\theta \, d\theta}{4\pi} \quad , \qquad (3 - 4)$$

$$\therefore \quad \bar{I} = \frac{2}{3} I_o \quad .$$

Thus for the radiating atom:

$$\bar{I} = \frac{2}{3}\left(I_z + I_x + I_y \right) ,$$

$$= \frac{2}{3}\left(I_z + 2I_x \right) . \qquad (3 - 5)$$

Consider the intensity of radiation at the point L in fig. 3:1, which lies in a direction making an angle θ with the Z axis, thus

$$I(\theta) = I_z \sin^2\theta + I_x + I_y \cos^2\theta$$

$$= I_z (1 - \cos^2\theta) + I_x (1 + \cos^2\theta)$$

$$= \frac{3\bar{I}}{2(I_z + 2I_x)} \cdot \left\{ (I_z + I_x) - (I_z - I_x)\cos^2\theta \right\} .$$

Dividing numerator and denominator by $(I_z + I_x)$ gives

$$I(\theta) = \frac{3\bar{I}\,(1 - P\cos^2\theta)}{3 - P} . \qquad (3 - 6)$$

At 90°, where most polarisation measurements are made,

$$I(90^\circ) = \frac{3\bar{I}}{3 - P} . \qquad (3 - 7)$$

Note that combining equations (3 - 2) and (3 - 5) leads to an alternative definition for the polarisation ,

$$P = \frac{6I_{//} - 3\bar{I}}{2I_{//} + 3\bar{I}} . \qquad (3 - 8)$$

The quantity $\bar{I}$ is a true average intensity, since when it is integrated over all solid angles it gives the total intensity. It is convenient, however, to define a quantity I_t as follows,

$$I_t = I_x + I_y + I_z . \qquad (3 - 9)$$

Thus $$I_t = \frac{3}{2}\bar{I} ,$$

and $$P = \frac{3I_{//} - I_t}{I_{//} + I_t} . \qquad (3 - 10)$$

3.2 The Atomic System

In fig. 3:3, $|o\rangle$ represents the ground state of the atom, and $|i\rangle$ is an upper state to which the atom may be excited by electron impact. The matrix element for a dipole along the ξ axis is $\langle o|\xi|i\rangle$, and the transition probability is

$$A_\xi(i) = c(\nu)\ |\langle o|\xi|i\rangle|^2 \qquad (3 - 11)$$

where $$c(\nu) = \frac{64\pi^4 e^2 \nu^3}{3 h c^3} \qquad (3 - 12)$$

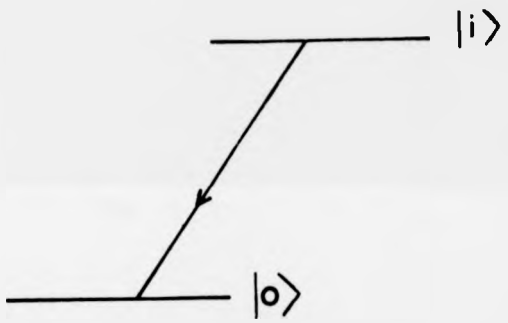

3:3

With reference to fig. 3:1, for radiation propagated along OY,

$$I_z = C\ n(i)\ A_z(i) \qquad (3 - 13)$$

$$I_x = C\ n(i)\ A_x(i) \qquad (3 - 14)$$

where C is a constant, and n(i) is the number of atoms in state $|i\rangle$. From equation (3 - 9),

$$I_t = I_z + I_x + I_y$$

$$= C\ n(i)\ A_t(i) \qquad (3 - 15)$$

where $$A_t(i) = \sum_\xi A_\xi(i)$$

Let the cross - section for excitation of the state $|i\rangle$ from the ground state $|o\rangle$ be Q(i), then if the electron velocity is v_e,

a rate coefficient K(i) may be defined by,

$$K(i) = v_e \, Q(i) \qquad (3 - 16)$$

Consider an electron density of n_e in the exciting beam of electrons. Then, in a steady - state condition, when the number of atoms entering the upper state is in equilibrium with the number of atoms decaying spontaneously back to the ground state,

$$n(i) \, A_t(i) = n_e \, n(o) \, K(i) \qquad (3 - 17)$$

where n(o) is the number of atoms in the ground state. Thus the rate of emission of photons coming from the ζ dipole is,

$$n(i) A_\zeta(i) = n_e \, n(o) \, K_\zeta(i) \qquad (3 - 18)$$

where $$K_\zeta(i) = \frac{A_\zeta(i)}{A_t(i)} \, v_e \, Q(i) \qquad (3 - 19)$$

Thus, equation (3 - 10) may be written in the form

$$P = \frac{3K_z(i) - K(i)}{K_z(i) + K(i)} \qquad (3 - 20)$$

Following Percival and Seaton[12], it is possible to express the rate coefficients in terms of the cross sections for excitation of the M_L sublevels of the upper state,

$$P = \frac{G(Q_0 - Q_1)}{h_0 Q_0 + h_1 Q_1} \qquad (3 - 21)$$

This is for an upper P state, and the subscripts refer to the M_L values of the levels concerned. Note that the cross - section for excitation of the $M_L = +1$ sublevel is the same as for the $M_L = -1$ sublevel. The method of calculating the constants G, h_0 and h_1 is given by Percival and Seaton, who show that the Oppenheimer - Penney theory is adequate, provided that the fine-structure and hyperfine-structure separations are not comparable with the line width. Otherwise a more complete theory must be used.

Fine-structure and hyperfine-structure affect the polarisation due to precessional effects. Specifically, for fine-structure, on the vector model, it is the precession of $\underline{L}$ and $\underline{S}$ about $\underline{J}$ which leads to a drop in polarisation from what would be expected in the absence of fine-structure. The effect is negligible only if the lifetime of the state is much shorter than the reciprocal fine-structure splitting frequency. Similarly, in the case of hyperfine-structure, it is the precession of $\underline{J}$ and $\underline{I}$ about $\underline{F}$ which leads to a further reduction in polarisation. In the case of mercury, the lifetime of the $^1P_1$ state is about 10^{-9}s, that of the $^3P_1$ state is about 10^{-7}s, whereas the hyperfine-structure splitting frequency is about 10^{10}Hz, and the fine-structure splitting frequency is about 10^{14}Hz. Clearly, it is necessary to include the effects of both fine- and hyperfine-structure for these states.

Percival and Seaton[12] have shown that the polarisation depends on the quantities ϵ and ϵ_J, where

$$\epsilon = 2\pi\delta\nu/A \quad , \quad \text{and}$$

$$\epsilon_J = 2\pi\delta\nu_J/A \quad .$$

Here, A is the radiative transition probability, and $\delta\nu$ and $\delta\nu_J$ are the fine- and hyperfine-structure splitting frequencies.

Flower and Seaton[56] have applied this analysis to the alkali resonance lines, and find that the calculated threshold polarisations are in good agreement with the measured values of Hafner, Kleinpoppen and Kruger.[16]

3.3 Application to the 6^1P_1 and 6^3P_1 Levels of Mercury

The Percival and Seaton theory has been applied to mercury by McConnell and Moiseiwitsch[28]. The mercury atom may be treated in a similar manner to helium, provided the core of 78 electrons is assumed not to interact with the two n = 6 electrons. The states concerned are initially formulated in LS coupling representation,

$$\psi(SLM_SM_L)$$

and are then transformed by the Clebsh - Gordan vector coupling coefficients into the J,M_J representation,

$$\psi'(SLJM_J) = \sum_{M_SM_L} C^{SLJ}_{M_SM_LM_J}\psi(SLM_SM_L) \qquad (3-22)$$

The $\psi(SLM_SM_L)$ may be split into two parts; the spatial, and the spin, wave functions.

$$\psi(SLM_SM_L) = \phi(SLM_L)\,\chi(SM_S) \qquad (3-23)$$

where

$$\phi(SLM_L) = \frac{1}{\sqrt{2}}\left\{ Y_{l_1m_1}(\theta_1,\phi_1)\frac{R_{n_1l_1}(r_1)}{r_1}\, Y_{l_2m_2}(\theta_2,\phi_2)\frac{R_{n_2l_2}(r_2)}{r_2} \pm Y_{l_1m_1}(\theta_2,\phi_2)\frac{R_{n_1l_1}(r_2)}{r_2}\, Y_{l_2m_2}(\theta_1,\phi_1)\frac{R_{n_2l_2}(r_1)}{r_1} \right\} \qquad (3-24)$$

where $Y_{lm}(\theta,\phi)$ is a spherical harmonic, and $R_{nl}(r)$ is a radial wave function. The subscripts 1 and 2 refer to the two electrons. These are the pure Russell - Saunders wave functions, which, although valid for helium, are only good as first approximations in the case of mercury, due to the important spin-orbit interaction, which leads to a partial breakdown of LS coupling, and a mixing of the 6^1P_1 and 6^3P_1 states. Note that the singlet spin function $\chi(00)$ is necessarily antisymmetric, which means that the singlet spatial wave function $\phi(01M_L)$ must be symmetric to make the total $\psi(^1P_1)$

antisymmetric. Therefore, the + sign in equation (3 - 24) refers to the singlet state, and the - sign to the triplet state.

The next step is to allow for the mixing of the 6^1P_1 and 6^3P_1 states, by writing

$$\psi(^3P_1) = a\psi'(^3P_1) + b\psi'(^1P_1) \qquad (3 - 25)$$

$$\psi(^1P_1) = a\psi'(^1P_1) - b\psi'(^3P_1) \qquad (3 - 26)$$

The normalisation is such that

$$a^2 + b^2 = 1 \qquad (3 - 27)$$

a and b may be determined from the relation,

$$\frac{b^2}{a^2} = \frac{T(^1P_1)}{T(^3P_1)} \left\{ \frac{\lambda(^3P_1 - {}^1S_0)}{\lambda(^1P_1 - {}^1S_0)} \right\}^2 \qquad (3 - 28)$$

where T is the lifetime of the state concerned. The lifetimes have been determined by many workers. Using the values given by Lurio[31],

$$T(^1P_1) = 1{\cdot}31 \times 10^{-9}\text{s}$$

$$T(^3P_1) = 1{\cdot}14 \times 10^{-7}\text{s}$$

gives

$$a = -0{\cdot}985$$

$$b = 0{\cdot}171$$

The wave functions for the upper states may now be written in the form

$$\psi(SLJM_J) = \sum_{j=1}^{4} c_j(SJM_J)\, w_j(M_J) \qquad (3 - 29)$$

where

$$w_1(M_J) = \phi(0,1,M_L)\,\chi(0,0)$$

$$w_2(M_J) = \phi(1,1,M_L-1)\,\chi(1,M_S)$$

$$w_3(M_J) = \phi(1,1,M_L)\,\chi(1,M_S)$$

$$w_4(M_J) = \phi(1,1,M_L+1)\,\chi(1,M_S)$$

The constants $c_j(SJM_J)$ will include the a and b coupling coefficients. The radial wave functions $R_{nl}(r)$ can be expressed as a sum of exponentials:

$$R_{00}(r) = r\left\{A_0 \exp(-a_0 r) + B_0 \exp(-b_0 r)\right\}$$
$$R_{10}(r) = r\left\{rA_0' \exp(-a_0' r) + B_0' \exp(-b_0' r)\right\}$$
$$R_{11}(r) = r^2\left\{A_1 \exp(-a_1 r) + B_1 \exp(-b_1 r)\right\}$$

The constants appearing in these equations are given by McConnell and Moiseiwitsch as:

$$A_0 = 1{\cdot}703,\ a_0 = 0{\cdot}839,\ B_0 = -0{\cdot}799,\ b_0 = 1{\cdot}973$$
$$A_0' = 2{\cdot}022,\ a_0' = 1{\cdot}211,\ B_0' = -2{\cdot}460,\ b_0' = 2{\cdot}691$$
$$A_1 = 0{\cdot}265,\ a_1 = 0{\cdot}562,\ B_1 = 0{\cdot}780,\ b_1 = 2{\cdot}249$$

in units of the Bohr radius, a_B.

The incident electron may be represented by a plane wave, $\exp(i\underline{k}.\underline{r}_3)$. Thus the product wave function for the atom plus exciting electron is : initially,

$$\Psi_i = \frac{1}{\sqrt{3}}\sum \psi(^1S_0)\ \exp(i\underline{k}_i.\underline{r}_3)\ \sigma_{m_s}(s_3) \quad , \qquad (3-30)$$

finally,

$$\Psi_f = \frac{1}{\sqrt{3}}\sum \psi(^{2S+1}P_{JM_J})\ \exp(i\underline{k}_f.\underline{r}_3)\ \sigma_{m_s'}(s_3) \quad , \qquad (3-31)$$

where the summation refers to the cyclical exchange of space and spin coordinates $\underline{r}$, s, which is necessary to antisymmetrise the wave functions. $\sigma_{m_s}(s)$ is the spin function for the free electron with spin quantum number m_s.

The total cross - section is now expressed in the form

$$Q = \frac{1}{2}\sum_{m_s m_s'} \frac{k_f}{k_i}\int_0^{\pi}\int_0^{2\pi} |f(\theta)|^2 \sin\theta\, d\theta\, d\phi \quad , \qquad (3-32)$$

where $f(\theta) = \frac{-a_B}{2\pi}\int \Psi_f\, V\, \Psi_i\, d\tau$, (3 - 33)

and $$V = \frac{1}{|\underline{r}_1 - \underline{r}_3|} + \frac{1}{|\underline{r}_2 - \underline{r}_3|} - v(r_3) \quad , \qquad (3-34)$$

where V is the interaction potential, and $\underline{r}_1$, $\underline{r}_2$ and $\underline{r}_3$ are the position vectors for the three electrons. $v(r_3)$ is the core potential

at a distance of r_3 from the nucleus.

The $f(\theta)$ may now be split into two parts: F, the direct scattering amplitude, and G_j, the exchange scattering amplitudes;

$$F = \int w_1 \, V \, \phi(0,0,0) \exp(i \, \underline{K}.\underline{r}_3) \, d\tau \quad , \qquad (3 - 35)$$

$$G_j = \int w_j \, V \, \phi(0,0,0) \exp(i \, \underline{k}_i.\underline{r}_3 - i \, \underline{k}_f.\underline{r}_1) \, d\tau \, , \qquad (3 - 36)$$

where $\underline{K} = \underline{k}_i - \underline{k}_f$.

Thus
$$Q(SJM_J) = \frac{a_B^2}{2\pi k_i^2} \int_{K_{min}}^{K_{max}} \left[\left| c_1 (F - G_1) \right|^2 + \sum_{j=2}^{4} \left| c_j G_j \right|^2 \right] K \, dK \, , \qquad (3 - 37)$$

where $K_{min} = k_i - k_f$,

$K_{max} = k_i + k_f$.

This is known as the Born - Oppenheimer approximation, and is valid provided weak coupling can be assumed between the initial and final states of the atom. This is probably justifiable since there is a large energy difference between the ground state and either of the 6P states. However, the Born - Oppenheimer approximation generally gives cross - sections too high. Use of the Ochkur[29] approximation often gives more consistent results. Only the first term in the interaction potential is retained for this approximation which thus leads to an easier calculation, as well as giving more reliable results.

Thus the interaction potential may be written

$$V = \frac{1}{|\underline{r}_1 - \underline{r}_3|} \qquad (3 - 38)$$

Noting that[32]

$$\frac{1}{4\pi|\underline{r}_1 - \underline{r}_3|} = \frac{1}{(2\pi)^3} \int \exp\left[i\underline{K}.(\underline{r}_1 - \underline{r}_3) \right] \frac{dK}{K^2} \qquad (3 - 39)$$

But, from a property of δ functions:

$$\delta(\underline{r}) = \frac{1}{(2\pi)^3} \exp(i\underline{K}.\underline{r})\, d\underline{K} \qquad (3-40)$$

Thus

$$\frac{1}{|\underline{r}_1 - \underline{r}_3|} = \frac{4\pi}{K^2}\, \delta(\underline{r}_1 - \underline{r}_3) \qquad (3-41)$$

Note that $\underline{K}$ is the momentum transfer, and that the main contribution to the exchange integral G_j will come from $\underline{k}_i$.

Equation (3 - 41) makes a great simplification to the evaluation of the exchange integral, one point being that the equation (3 - 36) is essentially a double integral over the coordinates of two electrons ($\underline{r}_1$ and $\underline{r}_3$). The δ function appearing in equation (3 - 41) reduces the exchange integral to

$$G_j = \int w_j\, \phi(0,0,0) \exp(i\,\underline{K}.\underline{r}_3)\, d\underline{r}_3 \qquad (3-42)$$

McConnell and Moiseiwitsch[28] present data for the cross - sections $Q(SJM_J)$ and use them to calculate the polarisation. Fig. 3:4 is a reproduction of their theoretical predictions for the polarisation of the $6^1S_0 - 6^1P_1$ and $6^1S_0 - 6^3P_1$ transitions.

Note that the effect of isotopic spin is included in the G, h_0 and h_1 coefficients in equation (3 - 21), and does not affect the cross - sections $Q(SJM_J)$. These coefficients are tabulated in table 3:1. The value of the polarisation at threshold is 0·77 for the 1850 A line and - 0·68 for the 2537 A line.

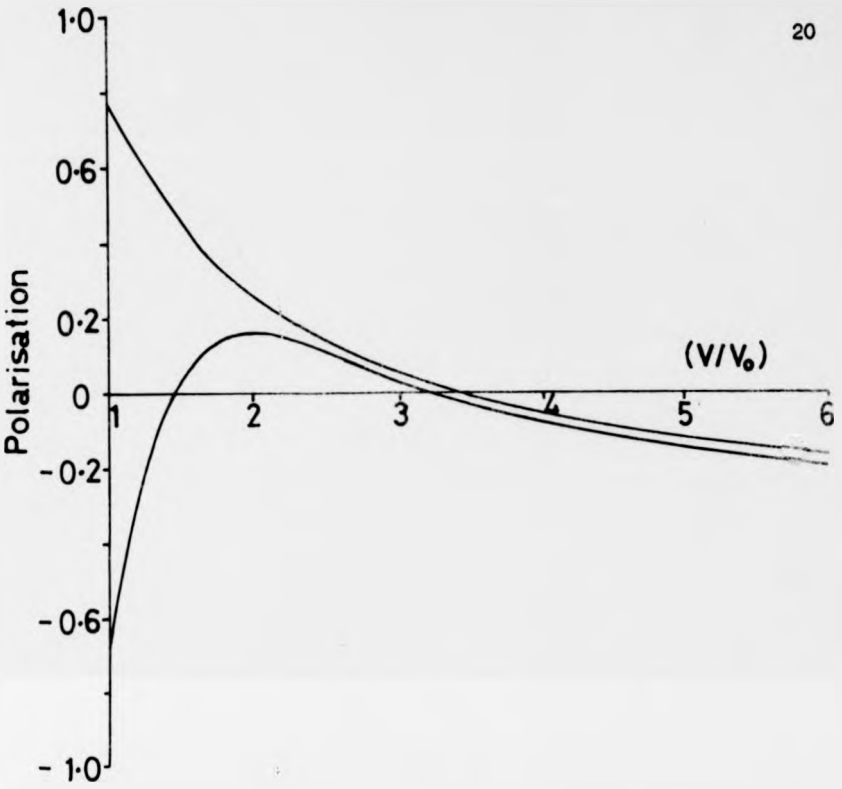

3.4 Polarisation of the 1850 A line (upper), and the 2537 A line (lower). The abcissa units are $(V/V_o)^{\frac{1}{2}}$, where V_o is the threshold energy for each line. (From McConnell and Moiseiwitsch.)

Table 3:1 Constants G, h_0 and h_1 in equation (3 - 21) for different nuclear spins, I. (From McConnell and Moiseiwitsch)

I	G	h_0	h_1
0	1	1	1
$\frac{1}{2}$	3	7	11
$\frac{3}{2}$	111	337	563

3.4 Simplified Expressions for Threshold Polarisation

Sometimes it is useful to be able to obtain a rough estimate of the threshold polarisation, without employing the complete formalism. In a similar manner to equation (3 - 22), the cross - section $Q(SLM_S M_L)$ may be transformed into the cross - section $Q(SLJM_J)$ by the relation (from Percival and Seaton[12])

$$Q(SLJM_J) = \left(C^{S\ L\ J}_{M_S M_L M_J}\right)^2 Q(SLM_S M_L) \qquad (3 - 43)$$

Since, at threshold, the outgoing electron can carry away no energy, it cannot remove any angular momentum either, and thus the threshold selection rule is arrived at

$$\Delta M_L = 0 \qquad (3 - 44)$$

Initially, $L = M_L = 0$, thus the only non - zero cross - sections will be $Q(SLM_S 0)$. Hence,

$$Q(SLJM_J) = \left(C^{S\ L\ J}_{M_S\ 0\ M_J}\right)^2 Q(SLM_S 0) \qquad (3 - 45)$$

But, $M_S + M_L = M_J$

$$\therefore\ Q(SLJM_J) = \left(C^{S\ L\ J}_{M_J\ 0\ M_J}\right)^2 Q(SLM_J 0) \qquad (3 - 46)$$

For the $6^1S_0 - 6^3P_1$ transition,

$$Q(1,1,1,\pm 1) = \left(C^{1\ 1\ 1}_{\pm 1\ 0\ \pm 1}\right)^2 Q(1,1,\pm 1,0)$$

$$= \tfrac{1}{2}\ Q(1,1,\pm 1,0) \ ,$$

and

$$Q(1,1,1,0) = \left(C^{1\ 1\ 1}_{0\ 0\ 0}\right)^2 Q(1,1,0,0)$$

$$= 0$$

Thus, when the 6^3P_1 state decays back to the ground state, only the transitions with $\Delta M_J = \pm 1$ will be possible, and these both give σ polarisation (as in the Zeeman effect), corresponding to a polarisation of - 1·0.

For the $6^1S_0 - 6^1P_1$ transition,

$S = 0$, and therefore $M_S = 0$.

Since $M_L = 0$, it follows that only the sublevel with $M_J = 0$ can be excited, and thus when radiative decay occurs, the only transition will be $\Delta M_J = 0$, which gives π polarisation, corresponding to a polarisation of + 1·0.

This very simple theory ignores spin - orbit interacion, and precessional effects.

4. Apparatus for the Vapour Experiment

4.1 General

The apparatus is shown schematically in fig. 4:1. The vacuum chamber, which had a volume of 3 litres, was constructed from Pyrex glass, with the exception of a Spectrosil window joined to the main vessel by several graded seals. The pump used was a 5 ls^{-1} mercury vapour diffusion pump, made from Pyrex glass, backed by a 50 ls^{-1} rotary pump (Edwards ES50). There was a small liquid nitrogen trap between the diffusion pump and the main chamber. The ultimate pressure obtainable with this system, after baking, was 1×10^{-6} Torr.

Mercury vapour was introduced into the vacuum from a small side - arm reservoir, which could be isolated when required by a diaphragm valve. The reservoir of mercury could be temperature controlled to within $2^{\circ}C$ in the range $-100^{\circ}C$ to $+80^{\circ}C$, using a Pye Ether controller. The reservoir was cooled by thermal contact with an aluminium cup, attached to a rod dipping into a dewar of liquid nitrogen, and was heated by a small bifilar - wound heating coil wound round the inside of the cup. The temperature was usually held near $0^{\circ}C$, when the pressure was measured to be 5×10^{-5} Torr with a Bayard - Alpert ionisation gauge, allowing for the calibration factor of 0·3 for mercury.

The vapour pressure was measured as a function of reservoir temperature (fig. 4:2). The measured points doe not lie on the saturated vapour pressure curve for two reasons. Firstly, at low temperatures, when the vapour pressure of mercury was less than 10^{-6} Torr, the residual gas partial pressure dominated. Secondly, the mercury vapour was never truly saturated due to the continuous pumping of the vacuum system, and perhaps because of a dirty

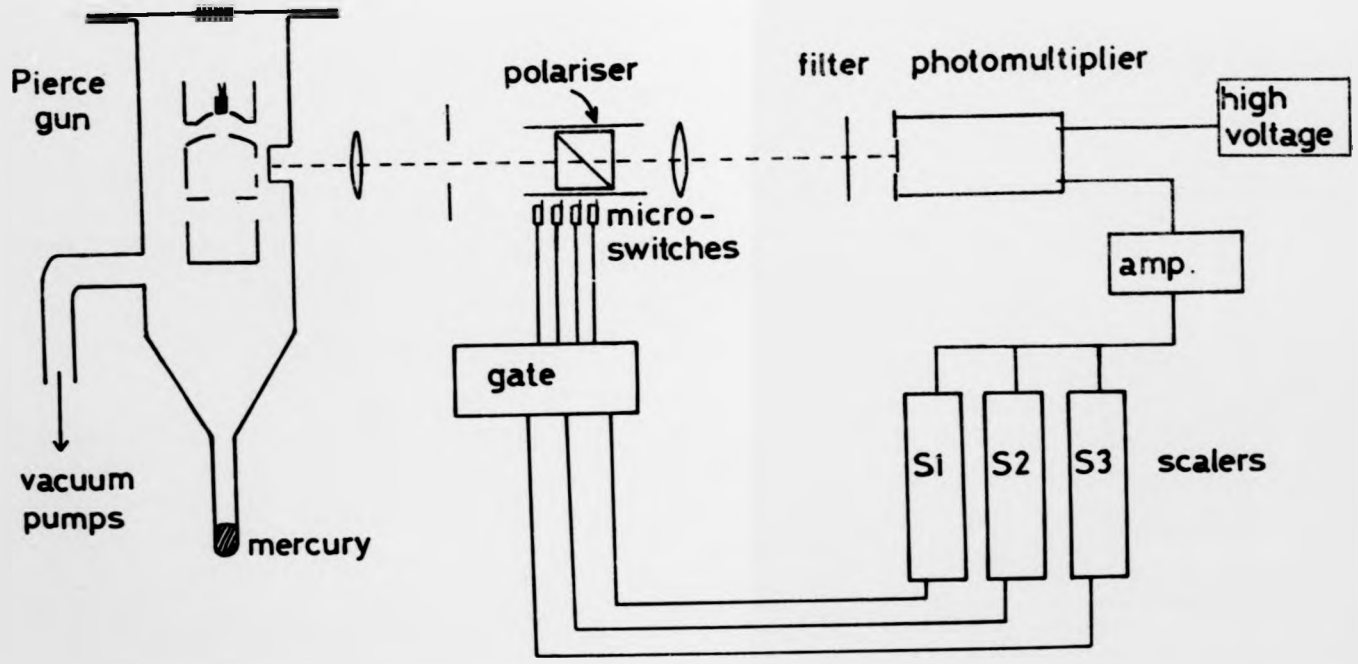

4:1 Schematic diagram of the apparatus used for the initial measurements of the 2537 A line

surface of the mercury. Thus the pressure was significantly lower than the saturated curve at higher temperatures. It was not possible to isolate the vacuum chamber to achieve saturation, owing to the outgassing of various surfaces, causing the residual gas pressure to rise too fast. The effect of mercury vapour on measured polarisation will be discussed later (section 5.2.1).

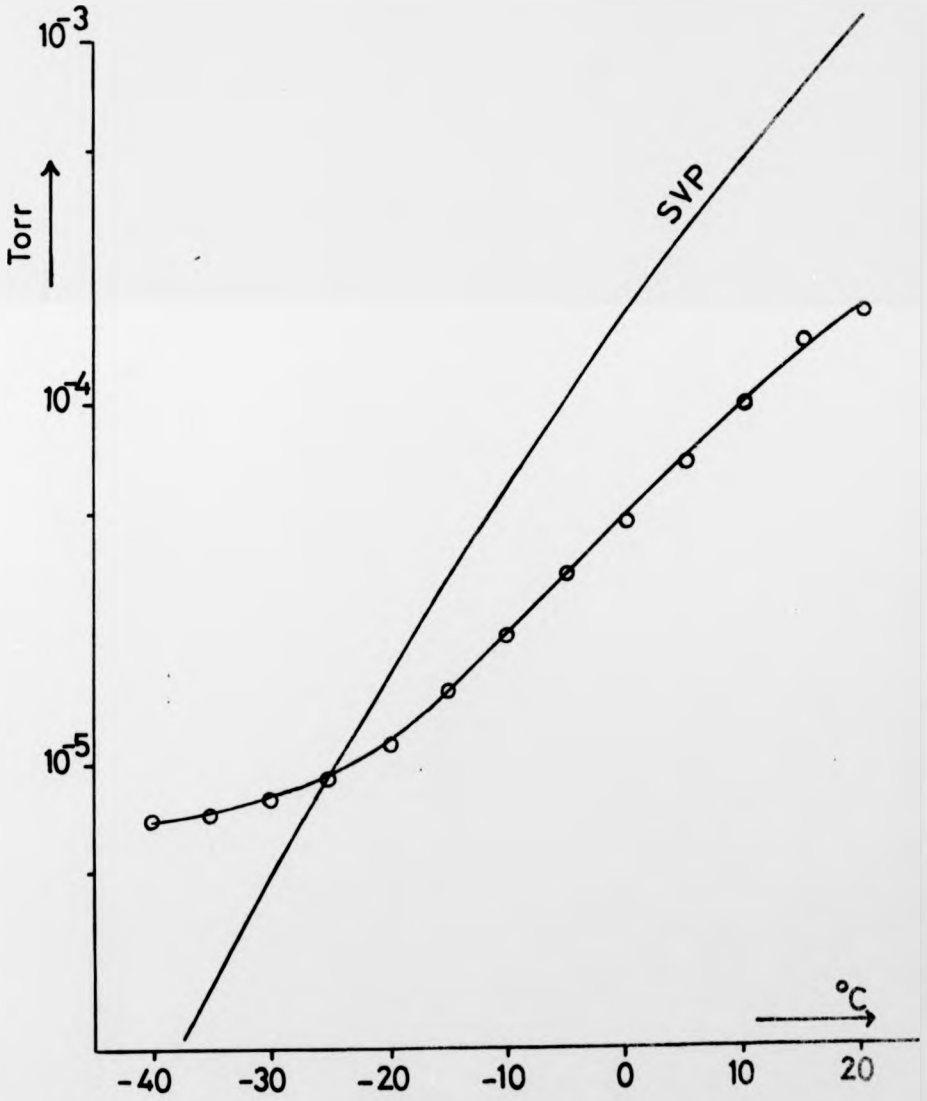

4:2 Pressure of mercury as a function of reservoir temperature

4.2 Electron Gun

The electron gun used in this part of the experiment was based on a Pierce system[30]. It is illustrated in fig. 4:3. It was constructed from non - magnetic stainless steel electrodes, supported on ceramic rods, and separated by glass spacers. The first electrode was held at the same potential as the cathode, and had a shaped surface, as did the anode, to try to achieve some focussing of the electron beam. The cathode was a Philips BP1A type, indirectly heated by a RCA spirally-wound heater. The cathode was held in by three pointed screws to reduce thermal losses. The interaction region was inside the anode; light emerging from this region passed through a small aperture in one side of the elctrode. The interior of the anode was blackened to avoid reflections. The aperture was about 3 cm away from the Spectrosil window in the vacuum chamber.

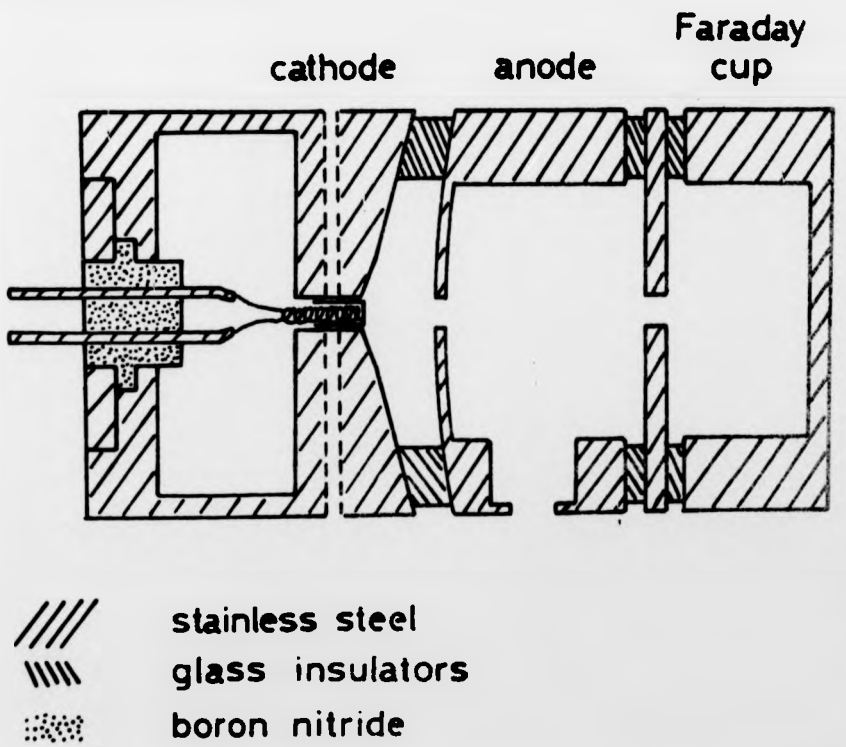

4:3 Diagram of the Pierce electron gun; supporting rods omitted.

At an electron energy of 5 eV, the current reaching the Faraday cup was typically 5×10^{-7}A. Although a Pierce - design gun should produce higher currents than this, a good energy resolution was obtained (250 - 300 meV). The electron beam divergence in the interaction region was measured to be $\sim 0{\cdot}3$ radians (full-angle), by replacing the usual Faraday cup with one consisting of several concentric electrodes, the electron beam divergence being calculated from the ratio of the collected currents.

No magnetic field was applied to compensate the earth's field. This caused a slight depolarisation of the emitted radiation due to precessional effects (see section 5.2.6).

4.3 Optics

All the optical components were constructed from Spectrosil, which transmitted down to 1700 A. The emitted radiation was collimated by a 20 cm focus lens, and then restricted slightly by an iris diaphragm. The radiation then passed through a Glan - Taylor polariser, which was rotated continuously at a constant frequency of $\sim 0{\cdot}5$ Hz. Only the ordinary ray was transmitted, and this was focussed on a 1st order interference filter, using another 20 cm focus lens. The filter transmitted at a centre wavelength of 2537 A, and had a FWHM of 150 A. The narrow convergence of the beam hardly affected the transmission of the filter, which was nearly 20%.

The radiation was detected by an EMI 6256S photomultiplier tube placed just behind the interference filter. This particular tube was chosen because of its very low dark current, combined with a medium gain. The quantum efficiency of the photocathode at 2537 A was 14%. The tube was cooled to 0°C by circulating a cold water/ glycerol mixture through copper tubing wound round the aluminium

housing containing the photomultiplier. The temperature was controlled to within 1°C. The effect of cooling was to reduce the dark current by a factor of about 20 compared with the value at room temperature. Fig. 4:4 shows the variation of dark current with temperature.

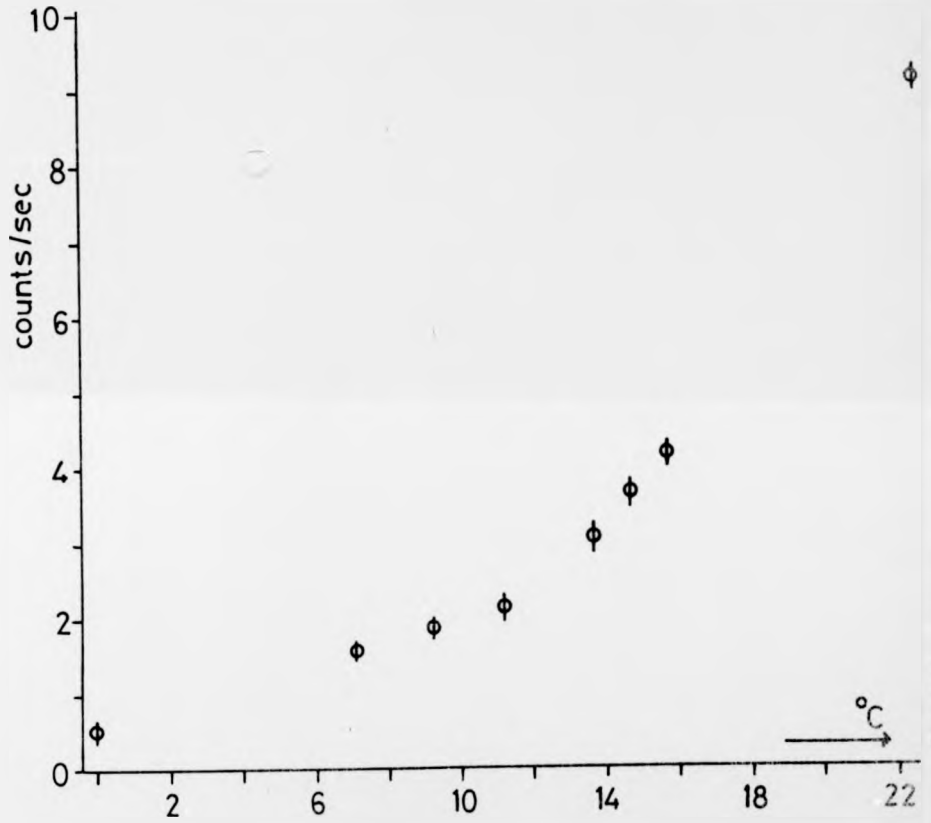

4:4 Variation of photomultiplier dark current with temperature. Error bars indicate 90% confidence limits.

The tube normally took 30 minutes to reach thermal equilibrium. Silica gel was used as a dessicant in the air space between the interference filter and the photomultiplier window, to prevent the latter

from becoming covered with condensed water vapour. Condensation was prevented from forming around the pins on the tube base by the same method. The outside of the tube, with the exception of the window, was coated with a conducting silver paint. This shield was connected to the cathode pin (which was held at ground potential) by a narrow strip of the same paint, and this prevented any build-up of charge on the interior of the glass envelope, which may have given rise to increased dark current.

The maximum signal-to-noise ratio recorded was 14:1 at the peak of the excitation function.

4.4 Electronics

The photomultiplier required 1400 V across its dynode chain for operation. The pulses, which were developed across a 2·2 kΩ resistor, were fed into an amplifier (NE 4603) via a 3000 pF isolating capacitor. After amplification and shaping, the pulses were analysed in a discriminator (NE 4602). The output pulses from this were fed simultaneously into three scalers, which will be denoted S1, S2, and S3. The scalers were gated on and off externally in the following manner. As the polariser rotated, four 'vanes' fixed on the outside of the tube containing the polariser sequentially depressed microswitch levers, in such a way that each microswitch was on for a quarter of a revolution. The microswitches operated a specially constructed gating unit, which contained 'anti-bounce' circuits to overcome any switching irregularities, and which gated the scalers in a selected sequence. The sequence was S1,S2,S1,S3. The orientation of the polariser was arranged so that the first polariser contained those counts arising when the plane of polarisation transmitted by the polariser was parallel to the electron beam direction, S2 when perpendicular, while during the period that S3 was gated on, the

electron beam was switched off, and this scaler recorded the dark current of the photomultiplier. After a preset number of revolutions, the gating sequence stopped, and the fractional polarisation could be calculated from the expression:

$$\bar{P} = \frac{\frac{1}{2} N1 - N2}{\frac{1}{2} N1 + N2 - 2N3} \times \frac{\pi}{2}$$

where N1 is the number of counts stored in S1, etc. The $\frac{\pi}{2}$ factor comes from the integral over the quadrants.

5. Results from the Vapour Experiment

5.1 Results

The method of gating the scalers, and computing the polarisation from the scaler readings is described in section 4.4. The relative excitation function ($I(90^\circ)$, see equation (3 - 7)) was obtained by finding $(\frac{1}{2} N1 + N2 - 2N3)$. Fig. 5:1 shows $I(90^\circ)$ and the polarisation P, both plotted as a function of the incident electron energy. The electron energy, as measured on a voltmeter, required a correction because of the effects of contact potential and space charge shifts.

The energy scale was normalised by placing the main peak of $I(90^\circ)$ at 5·6 eV. This value was taken from the measurement of Zapesochnyi and Shpenik[33], who, in their measurement of the excitation function of the 2537 A line, used an energy resolution of 100 meV. The resonance near 5·0 eV was observed, although with an instrumental resolution of nearly 300 meV, it was almost completely smeared out.

5.2 Sources of Error and Corrections

The following sources of error were considered:

1. Pressure depolarisation
2. Instrumental polarisation
3. Electron beam divergence
4. Finite solid angle of photon detection
5. Possibility of other lines being transmitted by the optical filter
6. Magnetic field depolarisation

5.2.1 Pressure Depolarisation

Photons emitted from the interaction region may be absorbed by mercury atoms before they pass through the window. If the density of mercury atoms along the optical path between the interaction region

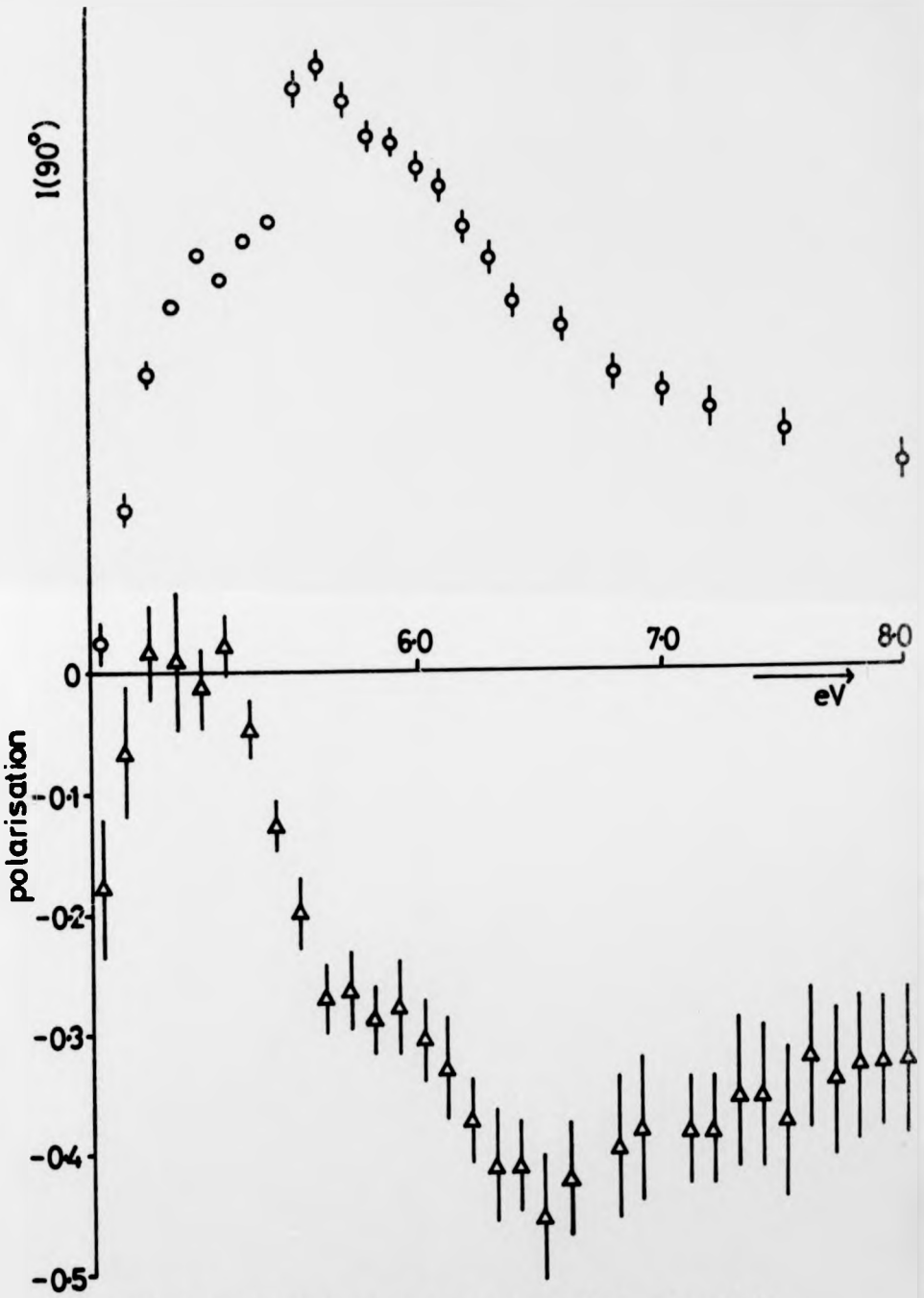

5:1 Relative excitation function and polarisation of the 2537 A line. Error bars indicate 90% confidence limits plus a small uncertainty in the systematic correction to the polarisation data.

and the window is sufficiently high, significant depolarisation of the resonance radiation will result. In the present experiment, the optical path length was 3 cm. The effect of this pressure depolarisation was assessed in the following way. The electron energy was kept constant, and the polarisation was measured as a function of the mercury vapour pressure. The result of this is shown in fig. 5:2.

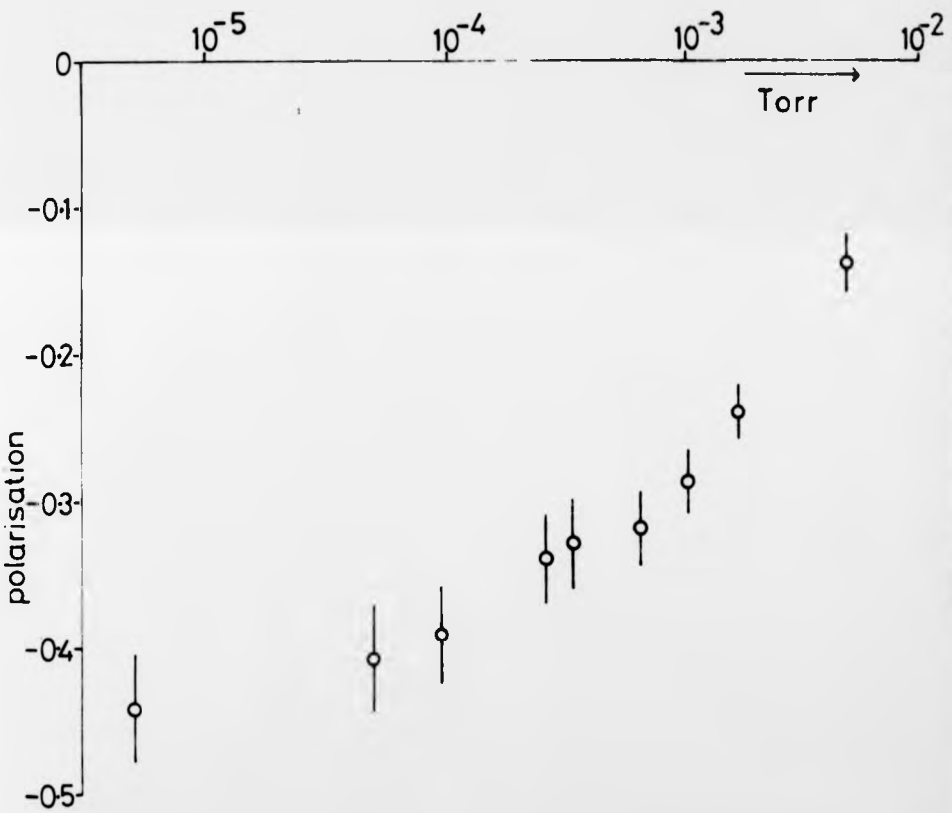

5:2 Pressure depolarisation of the 2537 A line. Error bars represent 1 standard deviation. There is a systematic uncertainty in the pressure measurements of approximately 20%.

There was an estimated uncertainty in the measurement of the pressure using a Bayard - Alpert ionisation gauge of about 20%. The error in the polarisation values was computed assuming Poissonian statistics. It will be seen that below 10^{-5} Torr, the depolarisation is small. Since the normal operating pressure was 5×10^{-5} Torr, a correction had to be applied to the measured polarisation data. The magnitude of this correction was 10% ± 5% of the polarisation.

5.2.2 Instrumental Polarisation

Suppose the apparatus used in measuring polarisation has a different sensitivity when detecting $I_{//}$ to when detecting $I_{\perp}$. These sensitivities will be denoted $S_{//}$ and $S_{\perp}$. Since the polarisation of the radiation is defined by

$$P = \frac{I_{//} - I_{\perp}}{I_{//} + I_{\perp}} ,$$

it follows that the apparent polarisation,

$$P' = \frac{S_{//}I_{//} - S_{\perp}I_{\perp}}{S_{//}I_{//} + S_{\perp}I_{\perp}} .$$

Let $$\pi = \frac{S_{//} - S_{\perp}}{S_{//} + S_{\perp}} .$$

π is usually referred to as the instrumental polarisation.

Let $$h = \frac{S_{//}}{S_{\perp}} , \quad \text{and } g = \frac{I_{//}}{I_{\perp}} .$$

$$\therefore P' = \frac{hg - 1}{hg + 1}$$

$$= \frac{h\,(1 + P)/(1 - P) - 1}{h\,(1 + P)/(1 - P) + 1}$$

$$= \frac{h + hP - 1 + P}{h + hP + 1 - P} ,$$

and, dividing by $(h + 1)$,

$$P' = \frac{(h - 1)/(h + 1) + P}{1 + P\,(h - 1)/(h + 1)}$$

$$= \frac{\pi + P}{1 + \pi P} .$$

The ΠP term in the denominator is often negligible.

The technique employed in measuring the instrumental polarisation was to construct a small light source which could be rotated by 90° about the axis of the detection optics. The source used was actually a panel - light bulb mounted in a specially made holder. This was placed at the position of the interaction region, and the apparent polarisation of it was measured before and after rotation by 90°.

If the polarisation of the source before rotation is P_s, then after rotation, this becomes $-P_s$.

The apparent polarisation before rotation is given by:

$P_1' = P_s + \Pi$, assuming Π to be small. After rotation this becomes

$$P_2' = -P_s + \Pi$$

$$\therefore \Pi = \frac{P_1' + P_2'}{2} \quad .$$

The two measured polarisations were:

$$P_1' = -0{\cdot}057 \quad ,$$

$$P_2' = +0{\cdot}010 \quad ,$$

giving $\Pi = -0{\cdot}024$.

As a further check, a piece of sheet polariser was placed in front of the light source, so as to deliberately make the source strongly polarised. The two measured polarisations were:

$$P_1' = -0{\cdot}257 \quad ,$$

$$P_2' = +0{\cdot}200 \quad ,$$

giving $\Pi = -0{\cdot}029$.

The mean of four such determinations was

$$\Pi = -0{\cdot}024 \pm 0{\cdot}006 \quad .$$

Inaccuracy with this measurement would arise if the light source was not placed exactly at the interaction region. This positioning

was difficult to check.

5.2.3 Divergence of the Electron Beam

The polarisation, P , of the radiation emitted by an atom excited by an electron travelling along the Z axis (see fig. 3:1), is related to the measured polarisation, P_m , of the radiation emitted from atoms excited by electrons moving in a range of trajectories lying within $\pm \alpha$ of the Z axis, by the relation

$$P = \frac{P_m}{(1 - \frac{3}{4}\alpha^2 + \frac{P_m \alpha^2}{4})}$$

This equation is derived in Appendix 1 (q.v.). Since the measured divergence of the beam was $\sim 0{\cdot}15$ radians (half - angle), the magnitude of the depolarisation for a measured polarisation of - 0·40 was 0·008. An uncertainty in the determination of the divergence angle of about 0·05 radians resulted in a systematic error in the polarisation values. This error was a function of the polarisation, and, for this reason, the error bars in fig. 5:1 include this uncertainty.

5.2.4 Solid Angle of Photon Detection

The polarisation, P , of the radiation observed along the Y axis only (see fig. 3:1), is related to the measured polarisation, P_m , of the radiation collected over a range in angle of $\pm \gamma$ to the Y axis by the equation

$$P = \frac{P_m}{(1 - \frac{\gamma^2}{4} + \frac{P_m \gamma^2}{4})}$$

This equation is derived in Appendix 2. The collecting lens used had a focal length of 20 cm, and an effective diameter of 4 cm. Thus

the angle δ was 0·1 radians. For a polarisation of - 0·40, the difference between P and P_m amounts to only 0·002, which was so much smaller than the other uncertainties of the data, that it was neglected.

5.2.5 Possibility of other lines being detected

There were several other Hg I lines within the bandwidth of the optical filter employed, but in every case the threshold for excitation was above 9·4 eV, and thus these were unimportant.

5.2.6 Magnetic Field Depolarisation

Refering back to fig. 3:1, in the absence of any magnetic field, the polarisation, here called P_o , is defined as

$$P_o = \frac{I_z - I_x}{I_z + I_x}$$

Suppose now that a weak magnetic field, H , exists in the direction OY. The radiating dipoles lying along OZ and OX at time t = 0, will precess about OY with an angular frequency, w , where

$$w = g_J w_L = 2\pi g_J f_L \quad ,$$

where f_L is the Larmor precession frequency, given by

$$f_L = \frac{e h}{2 m} = 1{\cdot}4 \text{ MHz/G}$$

For zero nuclear spin isotopes, g_J , the Landé g factor, is given by (see, for example, Woodgate[34])

$$g_J = g_L \frac{J(J+1) + L(L+1) - S(S+1)}{2J(J+1)} + g_S \frac{J(J+1) - L(L+1) + S(S+1)}{2J(J+1)}$$

where $g_L = 1$, and $g_S = 2$, to a very good approximation.

Thus $g_J\ (^3P_1) = \frac{3}{2}$

After a time t, both the OZ and OX dipoles will have precessed through an angle wt, and both I_z and I_x will have decayed in magnitude by a factor $e^{-\Gamma t}$, where Γ is the reciprocal lifetime of the state,

$$\Gamma = \frac{1}{T}$$

T, the lifetime, has been determined many times; a recent accurate value being $1{\cdot}17 \times 10^{-7}$ s (Dodd, Sandle and Williams[35]).

Thus, the measured intensity $I_{//}$ after a time t will be

$$I_{//} = (I_z \cos^2 wt + I_x \sin^2 wt)\, e^{-\Gamma t} \quad .$$

Similarly,

$$I_{\perp} = (I_x \cos^2 wt + I_z \sin^2 wt)\, e^{-\Gamma t} \quad .$$

$\int_0^\infty I_{//}\, dt$ gives the total number, $N_{//}$, of photons emitted by the system having E - vector parallel to the electron beam direction.

$$\therefore N_{//} = \int_0^\infty I_z \cos^2 wt\, e^{-\Gamma t} dt + \int_0^\infty I_x \sin^2 wt\, e^{-\Gamma t} dt \quad .$$

These integrals are evaluated by integrating twice by parts, giving

$$N_{//} = I_z \left(\frac{1}{2\Gamma} + \frac{\Gamma}{8w^2 + 2\Gamma^2}\right) + I_x \left(\frac{1}{2\Gamma} - \frac{\Gamma}{8w^2 + 2\Gamma^2}\right) \quad ,$$

with an analagous expression for $N_{\perp}$.

The measured polarisation is then given by

$$P = \frac{N_{//} - N_{\perp}}{N_{//} + N_{\perp}}$$

$$= \frac{(I_z - I_x)\left(\frac{\Gamma}{4w^2 + \Gamma^2}\right)}{(I_z + I_x)/\Gamma}$$

$$= \frac{P_o}{1 + 4\, w^2\, T^2} \quad .$$

Substituting $w = 1{\cdot}32 \times 10^7\ s^{-1}G^{-1}$, and $T = 1{\cdot}17 \times 10^{-7}$ s, gives

$$P = \frac{P_o}{1 + 9{\cdot}5\, H^2} \quad \text{where H is the field strength in Gauss.}$$

It should be noted that this formula only applies for a magnetic field along the direction of observation (OY). For a field along OX, the depolarisation effect is smaller, and for a field along OZ, there is no depolarisation. The effect will be different for isotopes with spin other than zero, but, as Mitchell and Zemansky[36] show, the above approximation is sufficiently good for most purposes. In the present experiment, the field strength along OY was 0·1 Gauss, giving

$$P = P_o / 1{\cdot}095$$

6. Apparatus for the Measurement of the 1850 A Line

6.1 The Crossed - beam Apparatus

For this measurement, a new crossed - beam apparatus was constructed. The vacuum chamber consisted of two tanks bolted together, which were constructed from non-magnetic stainless steel by Vacuum Generators Ltd., Sussex. The internal diameter was 350 mm, with various smaller side ports to take feedthroughs. A partition between the tanks created two chambers ; the oven chamber, and the interaction chamber.

The oven chamber contained only the mercury oven and its associated feedthroughs. A small aperture allowed the atomic beam to pass through into the interaction chamber, which contained the electron gun, mercury beam collector, mass spectrometer, window, ionisation gauge and electrical feedthroughs.

Mercury vapour diffusion pumps were used; an Edwards 6M3A, and a Leybold QUICK 505, both fitted with water cooled baffles, liquid nitrogen cold traps and butterfly valves. Both diffusion pumps were backed by one Leybold D12A rotary pump. The overall pumping speed of the system was $\sim 600\ ls^{-1}$. The ultimate pressure achievable in the interaction chamber was 2×10^{-7} Torr, although the normal background pressure, with the oven in the oven chamber, but not heated, was 2×10^{-6} Torr. The atomic beam was aligned with the horizontal axis of the tanks, the electron beam was vertical, and the excited radiation was observed in a direction orthogonal to both beams.

6.2 The Mercury Beam

This was produced by the oven/aperture system shown in fig. 6:1. The oven was constructed from non-magnetic stainless steel, and had a capacity of 50 ml. It could be heated to $150^{\circ}C$ by small heating rods, made by winding Kanthal wire around ceramic formers in a

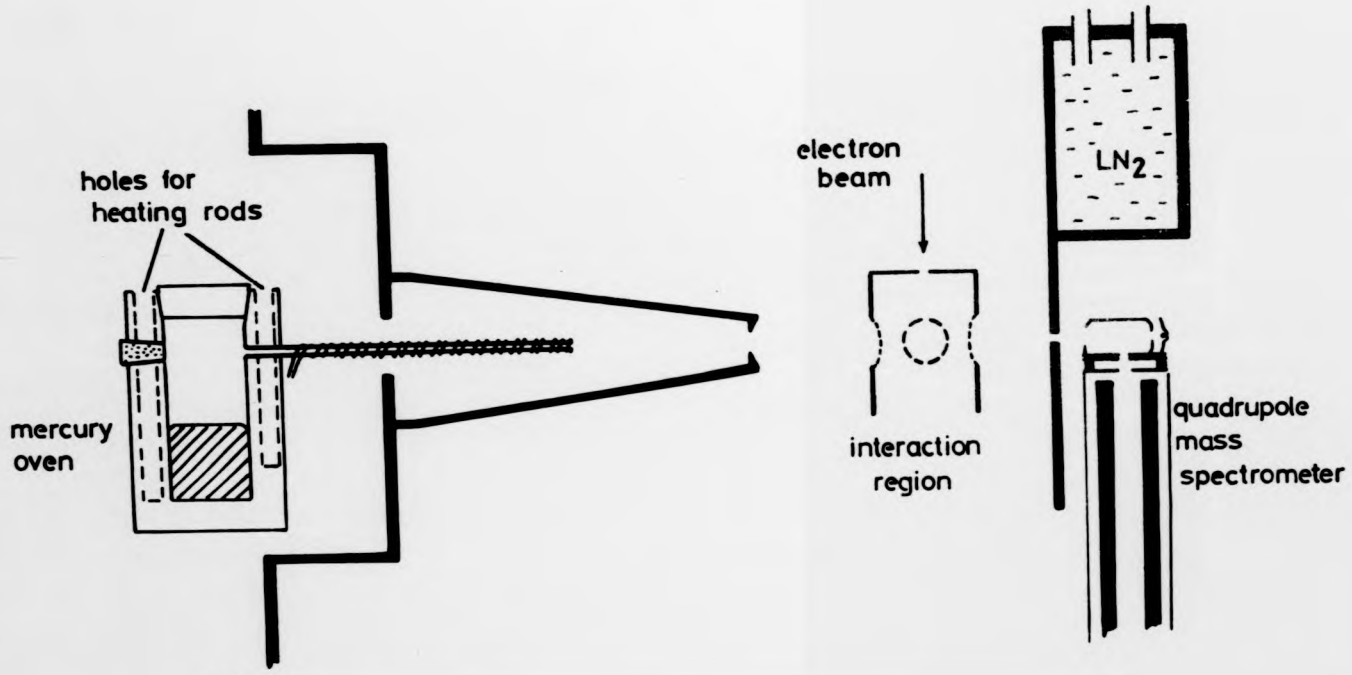

6:1 Schematic diagram of the mercury beam system. The glass feedthrough at the back of the oven is for the laser alignment of the system.

bifilar manner. These rods were then coated with a catephoric suspension of alumina to prevent shorting, and were inserted into holes in the main body of the oven. The aperture from the oven was a 1·7 mm bore ceramic tube, 80 mm in length. This was normally heated 25°C higher than the main part of the oven. Both the oven and tube temperatures were controlled to within 2°C, by means of Pye Ether controllers.

Usually, the oven was held at 125°C, and the tube at 150°C. It was found that these temperatures gave maximum stability of the atomic beam. In the tube, the vapour pressure was of the order of 1 Torr, and the mean free path of the atoms in this region would be ~0·1 mm. Thus the ceramic tube had only a small collimating effect, and served mainly to transport the mercury atoms to a point nearer the interaction region. Further collimation was provided by an unheated 2 mm circular aperture, spaced 50 mm from the end of the tube. The beam produced by this system passed through the interaction region, and was collected on a liquid nitrogen cooled surface. This prevented the pressure outside the beam from rising above 3×10^{-6} Torr. When the collector was allowed to warm up, however, the pressure rose to as much as 3×10^{-5} Torr, as measured with the Bayard - Alpert ionisation gauge. The cold plate had a small central hole to allow a small proportion of the beam through to a quadrupole mass spectrometer head. This was used to monitor the stability of the mercury beam. A short - term stability of ± 2% was found. The mass spectrometer was also used to check the isotope proportions of the mercury. These agreed well with the tabulated abundances for natural mercury.

6.3 The Two - stage Electron Gun

Fig. 6:2 is a diagram of the gun, which was based on a design of

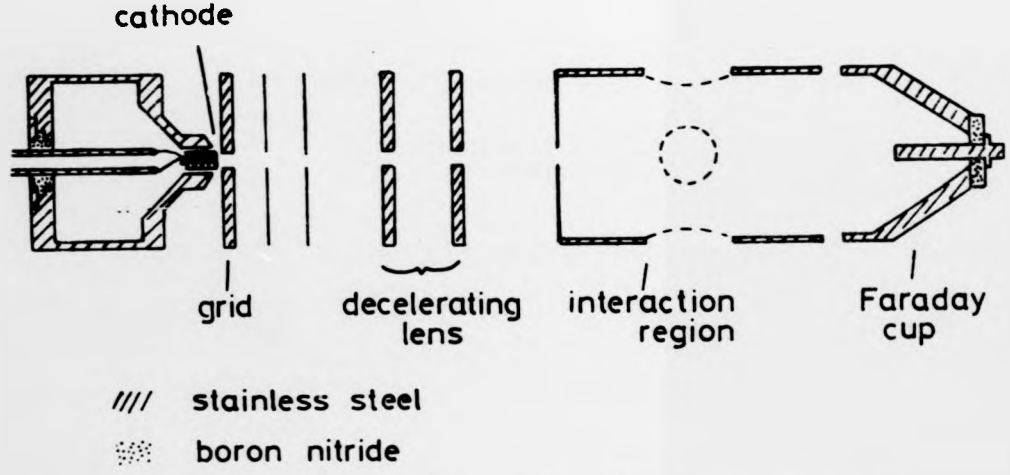

6:2 Diagram of the two-stage electron gun. Scale 1:1. The supporting rods are omitted for clarity.

Simpson and Kuyatt[37]. The first stage consisted of a Soa immersion lens, which extracted electrons from the cathode at a relatively high potential. The second stage was an aperture lens, which decelerated the electrons down to the final required energy.

The design was worked out from the following requirements. The operating voltage was to be ~7V (threshold for the $6^1S_0 - 6^1P_1$ transition), and the gun was to produce a final focussed spot of $\sim \frac{3}{4}$ mm diameter, at a distance of 23 mm from the last aperture, with a maximum convergence angle of 0·1 radians.

The usual space-charge equation to find the maximum current possible in such a system is[30]

$$I_{max} = 38{\cdot}6\ V_1^{3/2}\ a^2\ \mu A\ ,$$

where a is the convergence angle, and V_1 the final voltage. Thus, in this case $I_{max} = 7{\cdot}2\ \mu A$.

The current density at the focussed spot is given by

$$J_s = I_{max} \times \frac{4}{\pi d^2}\ ,$$ where d is the spot diameter.

Thus $J_s = 1640\ \mu A/cm^2$.

Then, following Pierce[30] (equation 8.10),

$$J_s = J_o(1 + \phi)\ \sin^2 a\ ,\ \text{with}\ \phi = \frac{11600\ V_1}{T}\ ,$$

where J_o is the current density at the cathode, and T is the cathode temperature (approximately 1100°K). Since a is small,

$$J_s \approx J_o\ (1 + 70)\ a^2$$

$$\therefore J_o = 2320\ \mu A/cm^2$$

Langmuir[38] gives the relation between current density extracted from the cathode, and the applied potential difference between the cathode and anode,

$$J_o = 2{\cdot}3\ V_o^{3/2}\ .$$

$\therefore V_o$ = 100 Volts , approximately. This fixes the deceleration ratio as about 15:1.

For the second stage lens, a bore of 10 mm was chosen, with the spacing also being 10 mm. The image distance, measured from the low voltage side of the lens was set at 40 mm. Using fig. 6:3 (from Spanenberg[39]), it is seen that this corresponds to an object distance of ~35 mm, and a magnification of about 1.

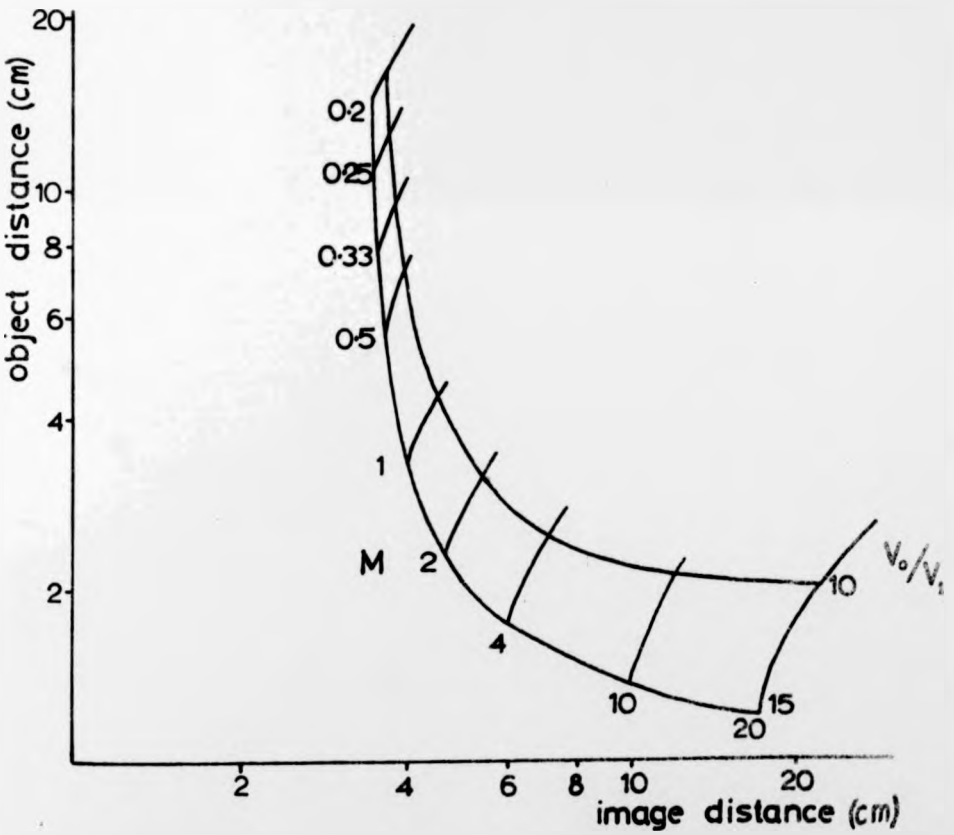

6:3 Aperture lens characteristics for a 10:1 and 15:1 decelerating lens (from Spanenberg[39]). Image and object distances to be measured from the low voltage side of the lens.

To design the first stage, it is necessary to find the perveance, p,

$$p = I/V_o^{3/2} \quad \text{, which gives}$$

$$p = 7 \times 10^{-3} \quad A/V^{3/2} \quad ,$$

and, from Simpson and Kuyatt[37], who give the properties of a standard Soa lens, this leads to a magnification of about 1 of the emitting area of the cathode, and an image distance of 14 times the cathode to grid spacing. This spacing was made as small as possible, $\sim 0{\cdot}3$ mm, giving the distance to the intermediate image as about 4 mm, to be measured from the anode. The area of emitting surface of the cathode is about half the grid bore in such a design, and since the grid bore was chosen to be 2 mm, this fixed the final image size as approximately 1 mm.

When the gun was operated, it was found that the first stage voltage had to be increased to about 150V to get the best focussing. The current reaching the Faraday cup was up to 6 μA for 7 eV electrons, and was reasonably stable, although there was some trouble with a non-conducting film (of cracked rotary pump oil ?) building up on the grid, leading to a reduction in the current. This electrode had to be occasionally cleaned in concentrated nitric acid to remove the film.

The energy spread of the electron beam was measured to be ~ 400 meV, by measuring the relative excitation function of the 2537 A line, the onset of which is so steep as to be considered instantaneous for energy-widths above about 100 meV.

The Faraday cup had a rod in the middle of it, to which the current flowing could be measured separately, giving a rough idea of the divergence of the electron beam at that point. From the ratio of the current collected in the main part of the cup, to the current

collected on the rod, a divergence of ~8° full angle was deduced.

All the electrodes were made from non-magnetic stainless steel, mounted on ceramic rods. As before, the cathode was a Philips BP1A type.

6.4 Optics

Fig. 6:4 is a diagram of the optical arrangement used for this measurement. The radiation was collected by a Spectrosil lens of 57 mm focal length and 25 mm effective diameter. The transmission was measured to be 80% at 1850 A using a scanning spectrophotometer. The lens was placed so that the interaction region was at its focus. This proved difficult to do, because the focal length (nominally 70 mm in the visible) is a rapidly varying function of wavelength in the ultraviolet part of the spectrum. However, a 1st order interference filter was available (supplied by Rofin Ltd.), which had a maximum transmission of 12% at 1850 A. Although this was not suitable for the detection of the line itself, since the transmission at 2537 A was not negligible, it was valuable for setting - up purposes, and using it, the focal length of the lens was measured at 1850 A. To do this, a mercury vapour discharge lamp was set up inside a glove box, which was continuously flushed with dry nitrogen to displace oxygen, which absorbs strongly at 1850 A. The filter was placed in front of the lamp, and an image of the discharge was formed with the lens on a flourescent screen. The object and image distances were measured, and the focal length was deduced to be 57 mm. The focal length was also calculated from tabulated values of the refractive index of Spectrosil to be 57·5 mm.

Several fluorescent screens were tried, but the most effective was made by spraying a saturated solution of sodium salicylate on

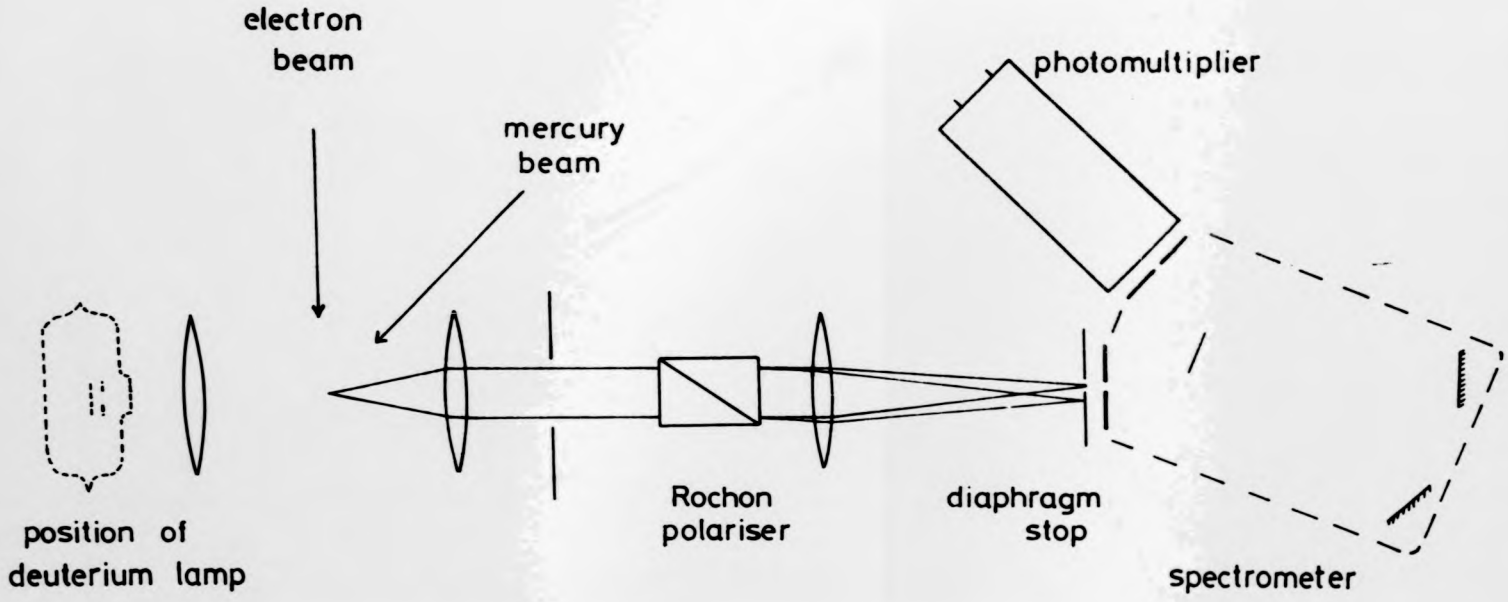

6:4 Schematic diagram illustrating the optical arrangement used for the polarisation measurements on the 1850 A line.

a glass slide or coverslip, and allowing to dry. After several coatings, a bright blue image could be obtained.

The collecting lens also served as a window, being sealed by a Viton o-ring. The nearly parallel beam of light emerging from the lens passed through a diaphragm stop of 12 mm diameter, and then through the polariser. This was of the Rochon type, made by B.Halle from synthetic crystal quartz, transmitting down to 1650 A. The Rochon design of polariser is similar to the Wollaston, in as much as both the ordinary and extraordinary rays are transmitted, with only a narrow divergence angle between them - in this case $1{\cdot}5^{\circ}$. The ordinary ray is undeviated in passing through the prism. The extinction ratio was 10^{-5}. The polariser was rotated at a constant frequency of 0·24 Hz.

The problem of separating the two beams of light emerging from the polariser was solved by placing a 160 mm focal length lens after the polariser, and focussing both beams down to images of the interaction region. The separation, d , of the two images, is given approximately by the relation $d = \theta f$,
where θ is the angle between the two beams, and f is the focal length of the lens. In this case, d = 4·2 mm.

The separation was checked experimentally by switching on the deuterium lamp (position shown in fig. 6:4) which acted as a virtual light source placed at the interaction region. Then, with the filter in position, the two images formed by the lens placed after the polariser were allowed to fall on a sodium salicylate fluorescent screen, and the two spots of visible light were photographed with a Polaroid camera. The separation of the spots was measured to be 4·2 ± 0·2 mm, in excellent agreement with the calculated value.

Since the radiation passing through the polariser was paraxial, the magnification of the optical system is simply given by

$$M = F2/F1$$

where F1 is the focal length of the collecting lens, and F2 is the focal length of the imaging lens.

Thus $M = 2{\cdot}9$

It was essential to avoid any overlapping of the two final images, or a reduction in the measured polarisation would have resulted. Therefore, the maximum image size allowable was 4·2 mm, which in turn fixed the maximum object size to be ~1·4 mm. This limiting of the amount of the interaction region which was visible to the detection optics was achieved by spot-welding a small cone made of thin sheet non-magnetic stainless steel into an aperture in the side of the cylindrical electrode (see fig. 6:2). The small hole in the apex of the cone was made 1·3 mm diameter. The whole of the electrode, and both surfaces of the cone were covered with soot to prevent reflections of the emitted radiation.

The two images formed by the imaging lens were allowed to fall on an adjustable iris diaphragm, the aperture of which was set to about 2 mm, thus being quite certain of passing only the ordinary beam through to the spectrometer behind.

The wavelength was isolated in a McPherson 218 grating spectrometer, in which the grating used was ruled with 2400 lines/mm, and was blazed at 3000 A. The slit width used was 2 mm on both the entrance and exit slits. Since the dispersion of the grating was 13·3 A/mm, the overall resolution achieved was ~27 A. This was checked experimentally by scanning over the line, and finding the FWHM of the line shape obtained. The result of this was ~25 A. The nearest line likely

to interfere with the measurement was the 1950 A quartet of Hg II. The 1850 A line was observed in both 1st and 2nd order. Although the line was marginally stronger in 2nd order, because the blaze wavelength was nearer, a neighbouring mercury line at 3704 A prevented this method from being used. After the exit slit of the spectrometer was a gas cell, through which dry nitrogen gas was circulated, and behind that was the photomultiplier.

The photomultiplier was the same one as used before in the vapour experiment (see p. 27), but the cooling arrangement was different. The cathode end of the tube was enclosed in a copper block, which was cooled on its four external flat faces by Peltier cooling modules, supplied by Mectron (Frigistor) Ltd. The 'hot' face of each module was in thermal contact with a water jacket. A current of 5·0 A in the modules produced a cooling of the photomultiplier down to - 20°C in about 20 mins. This led to a reduction in dark current by a factor of 20 - 25 over the value at room temperature (i.e. less than 0·5 count/s when cooled). The short term stability of the photomultiplier temperature was $\pm$ 0·5°C. The magnetic field produced by the current in the Peltier modules had no detectable effect on the performance of the photomultiplier.

Silica gel was used to prevent condensation forming on the pins of the tube, and on the window.

Dry nitrogen gas had to be circulated around all the optics due to the high absorption of oxygen at 1850 A. One of the rotational states of molecular oxygen lies near this wavelength[40], and the coefficient of absorption is ~ 1 cm^{-1}. It was found that unless the nitrogen was circulated continuously, the 1850 A line was not

visible at all, even though great care was taken to eliminate leaks in the optics housing. Evacuation of this part of the system was not possible owing to a curious effect this had on the dark current of the photomultiplier; the dark current rose by a factor of about 5. No satisfactory explanation was found for this effect.

Great care was taken to avoid reflection of the radiation from any surface. Likely surfaces were covered with a layer of soot, produced by igniting a mixture of benzene vapour and town gas.

6.5 Electronics

These were essentially the same as used in the vapour experiment (see p. 29), but the method of providing signals for gating the scalers was different. Four reed switches were placed symmetrically round the outside of the rotating tube containing the polariser. A magnet attached to the tube caused each switch in turn to stay on for a quarter of a revolution. It was possible, by making slight adjustments to the positions of the reed switches to get the four gating periods almost exactly equal in length.

7. Results from the 1850 A Line Measurement

7.1 Results

One of the main problems in determining the polarisation of this line was lack of intensity, which was mainly brought about by the inefficiency of the detection system. The transmission of the lenses and the polariser was only 70 - 80%, the spectrometer introduced another loss of intensity. Also, only a small part of the interaction region could be observed, and there may have been residual oxygen in the optics housing. These factors combined to give low count rates. For measurements of the relative excitation function, the signal could be improved by removing the polariser and the imaging lens, and moving the spectrometer nearer to the collecting lens. With the system thus simplified, it was also possible to get a more efficient nitrogen flushing system.

The upper part of fig. 7.1 shows the result of measuring the relative excitation function, $I(90^{o})$, in this way. Since the current through the electron gun was a function of the electron energy, the intensity plotted as ordinate was actually (signal - noise)/current. The energy scale required careful calibration. The method used was to tune the spectrometer to 2537 A, and to scan through the excitation function of that line, by applying a slow voltage ramp to the cathode of the electron gun, and feeding the analogue output of a ratemeter (NE 4607) to a chart recorder. The resonance at 5·0 eV (actually 4·92 eV, see section 9) was located to $\pm$ 0·05 eV by this technique. The voltage was measured with a digital voltmeter (Fenlow 701). This placed the threshold of the 1850 A line at 6·7 $\pm$ 0·1 eV. As a further check, the threshold regions of three other lines of mercury: 4046 A ($7^{3}S_{1} - 6^{3}P_{0}$) , 4078 A ($7^{1}S_{0} - 6^{3}P_{1}$) and 4358 A ($7^{3}S_{1} - 6^{3}P_{1}$)

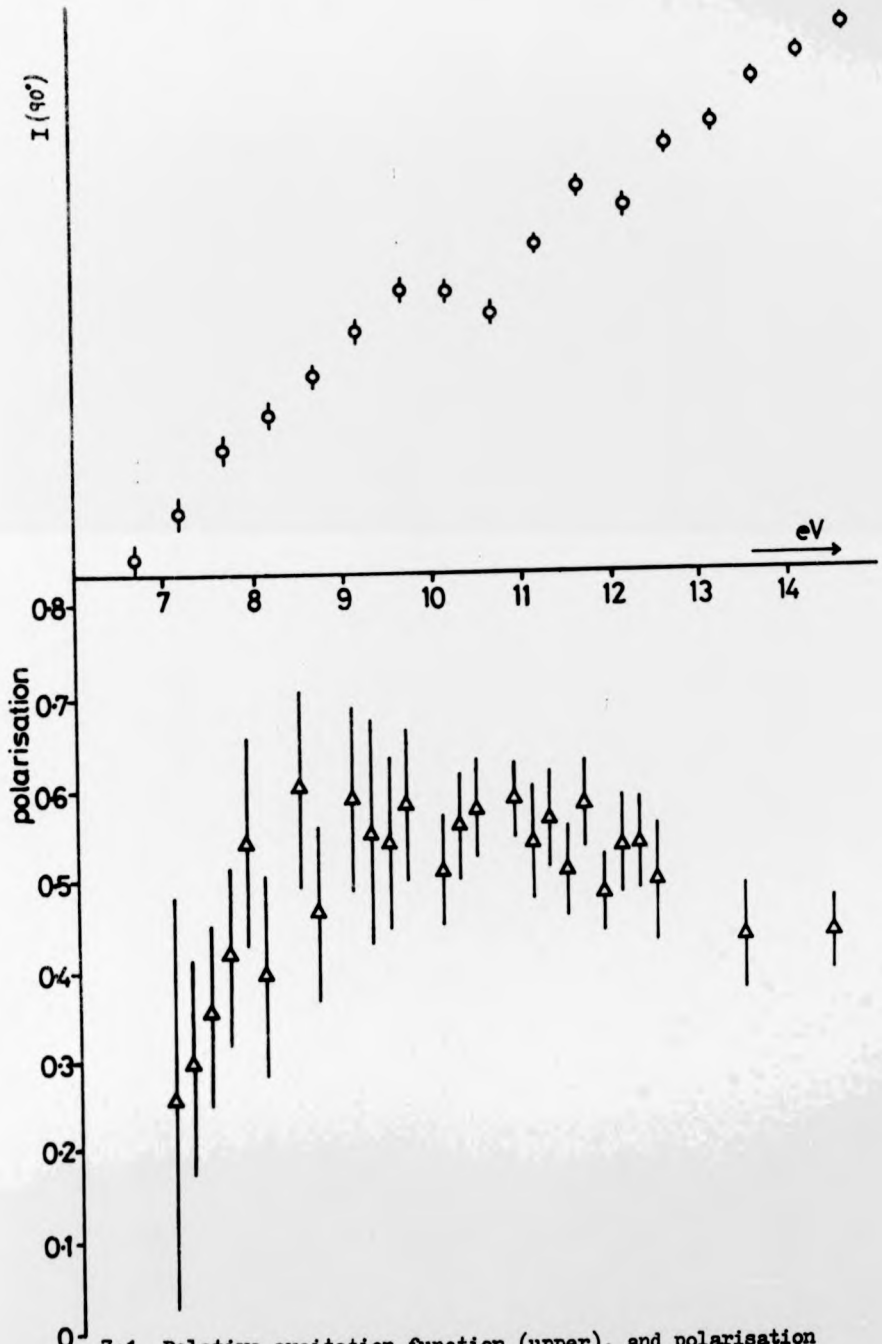

7:1 Relative excitation function (upper), and polarisation of the 1850 A line. Error bars indicate 90% confidence limits, plus a systematic error not exceeding 0·04 in the polarisation.

were scanned through in a similar manner, and, knowing the energy of the upper level of each transition, the threshold of the 1850 A line was again determined. In each case, the results were in agreement to within 0·1 eV. For a further discussion of the calibration of the energy scale, see section 10.3.1.

The lower part of fig. 7:1 shows the measured polarisation of the line, plotted on the same energy scale as $I(90^{o})$. These data are the average of several runs. Before each run, the energy scale was calibrated by using the 5·0 eV resonance in the 2537 A line, as described above. Because of the low count rates, however, a complete run through the energy range of 7 - 15 eV took several hours, during which time a slight energy shift of up to 0·5 eV sometimes occurred. Thus, although the accuracy of the polarisation was improved by averaging, the energy resolution was actually degraded to about 1 eV. On any particular run, the small dip in the polarisation at 10 eV showed more clearly than in the plotted data. The polarisation was not measured below 7·0 eV, due to the very low count rate in that region.

As a check that there were no serious unwanted reflections, the electron energy was kept constant, and the photomultiplier pulses were fed, via an amplifier and discriminator, into the input of a multichannel scaler. One of the gating pulses from the gating unit was used to trigger the beginning of the channel sweep, so that as the polariser rotated, the channel number of the multichannel scaler advanced until the polariser had made one complete revolution, when the sequence started again. After about 1 hour, a sinusoidal variation in the scaler contents was observed. This is plotted as a function of polariser angle in the polar diagram fig. 7:2. The expected pattern is that produced by a pair of crossed radiating dipoles, and as such,

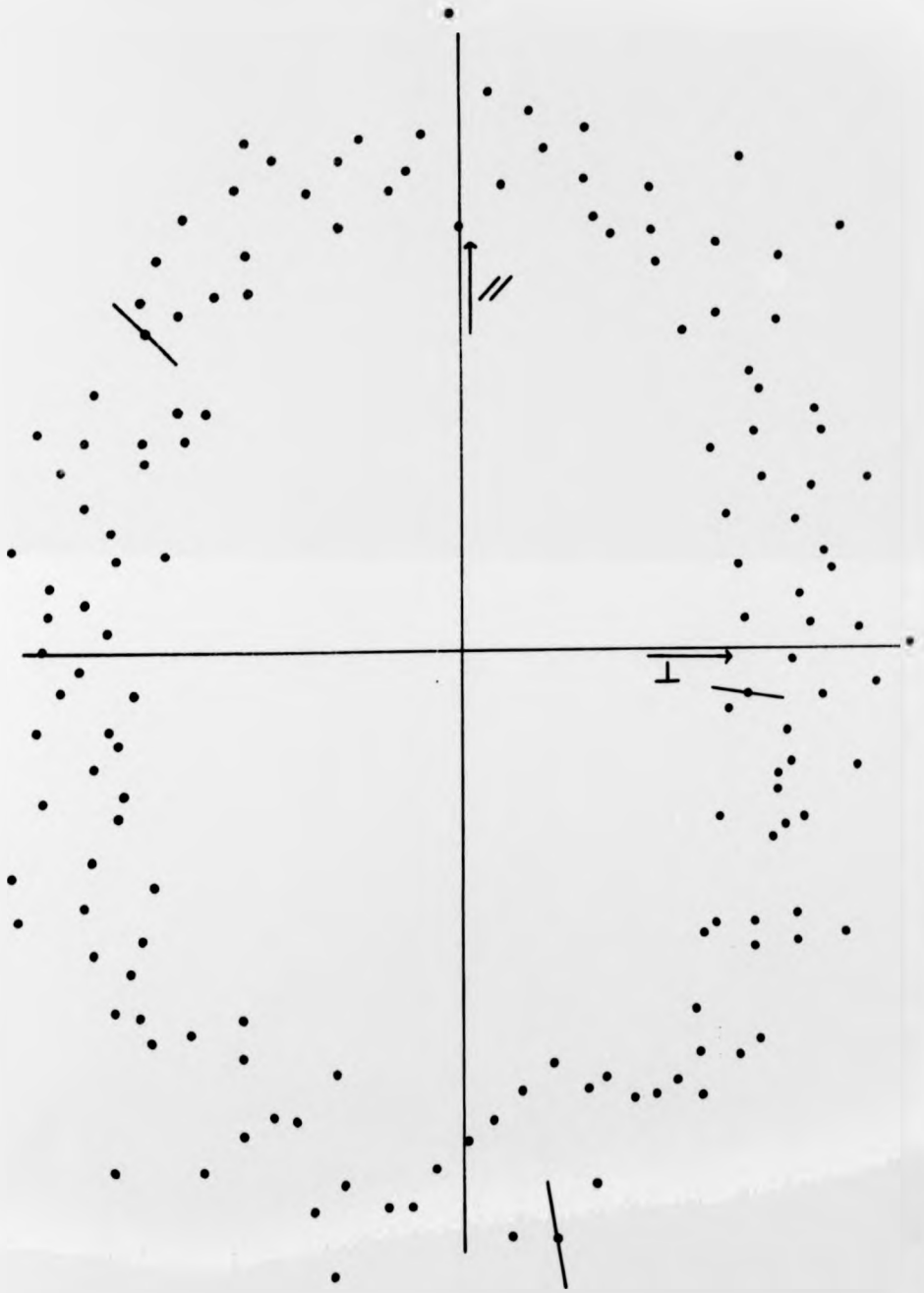

7:2 Polar diagram showing the intensity of transmitted radiation as a function of polariser angle.

should be symmetric. No serious asymmetries are apparent.

7.2 Errors and Corrections

The same sources of error as in section 5.2 were again considered.

7.2.1 Pressure Depolarisation

One of the advantages of the atomic beam technique is that the interactions take place in a region of relatively high atomic density, but the surrounding regions have a much lower density. To a large extent this eliminates the problem of pressure depolarisation since the amount of radiation trapping becomes small. This was indeed found to be the case; the polarisation was independent of the oven temperature (and hence the beam density) provided the beam collecting plate was kept cold. If the collector was allowed to warm up, however, atoms scattering off the surface of it without 'sticking' caused the background pressure in the interaction chamber to rise to about 2×10^{-5} Torr or higher. Under these circumstances, the polarisation was found to be a function of the pressure of mercury in the interaction chamber, the pressure being measured with a mass spectrometer, and also a function of the oven temperature. Fig. 7:3 shows how the measured polarisation at a fixed electron energy of 17 eV varied with the ion current in the mass spectrometer. It can be seen that if the atomic beam is not collected, then a definite depolarisation results.

7.2.2 Instrumental Polarisation

To determine this, radiation from the deuterium lamp was focussed into the interaction region with a 7 cm focal length lens (see fig. 6:4). The electron gun was removed, and a small quartz cell was placed at the precise position of the interaction region. This cell was filled with finely sintered quartz (Spectrosil), and a blackened disc of

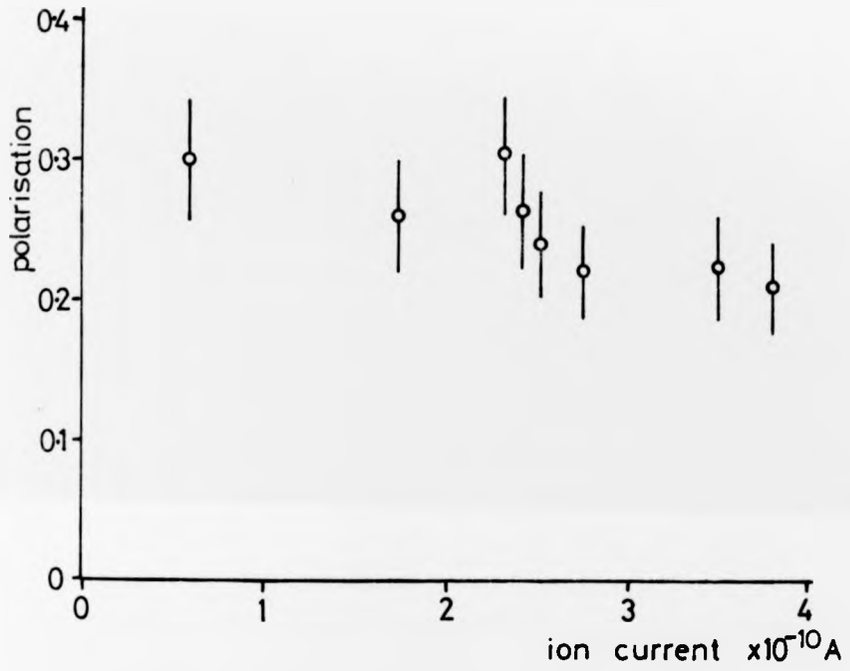

7:3 Polarisation of the 1850 A line as a function of mass spectrometer ion current.

sheet stainless steel with a 1 mm central aperture was attached to the side of the cell nearest the detection optics. This arrangement acted as a source of unpolarised radiation. The depolarising properties of the sintered quartz cell were checked in the visible, by placing it between two linear polarisers. No change in intensity was observed when the second polariser was rotated relative to the

first one. Thus the cell was capable of depolarising completely polarised light. Since the deuterium lamp could be expected to have very little polarisation in any case, it was concluded that the arrangement described above created a completely unpolarised source of radiation.

The cell transmitted so little radiation, however, that the apparent polarisation of the radiation was not measurable for wavelengths right down to 1850 A. Instead, the instrumental polarisation was measured for several wavelengths, and then extrapolated, see fig. 7:4.

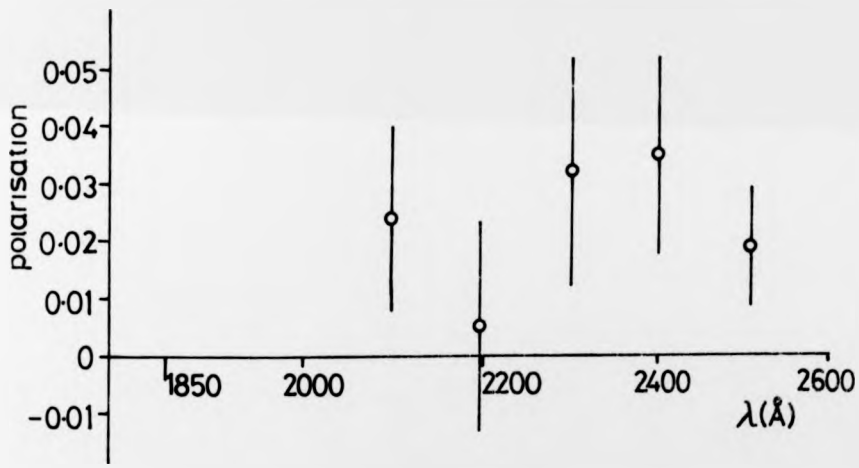

7:4 Instrumental polarisation as a function of wavelength. Error bars indicate 90% confidence limits.

There is no obvious trend in the data, and a least squares fit to a straight line yields a value of 0·02 at 1850 A. This method of extrapolation is not necessarily valid, however, and an error of ± 0·02 was assigned to this figure.

The most probable source of instrumental polarisation was the spectrometer, since this involves three reflections. The polarisation of the same model spectrometer has been determined in the ultraviolet by Matsui and Walker[41], and for longer wavelengths by Poulsen[42]. The former measured the polarisation at 1850 A to be - 0·05. At longer wavelengths, the spectrometer becomes strongly polarising. The polarisation depends to some extent on the age and condition of the grating.

7.2.3 Other Sources of Error

The polarisation data were corrected for the effects of electron beam divergence and finite solid angle of photon detection (see section 5.2) No other lines from Hg I were within the bandwidth of the spectrometer.

8. High Resolution Study of the 2537 A Line

8.1 General

The apparatus was the same as used for the measurement of the 1850 A line, except that the two-stage gun used for that line was replaced by an electron monochromator, and certain modifications had to be made to the optical arrangement and the electronics.

8.2 Monochromator

The monochromator was of the 127° cylindrical geometry type, and was made to a design of Raible[43], which was based on Marmet and Kerwin's design[44]. The device is sketched in fig. 8:1. The electrodes were made from oxygen - free copper, insulated from each

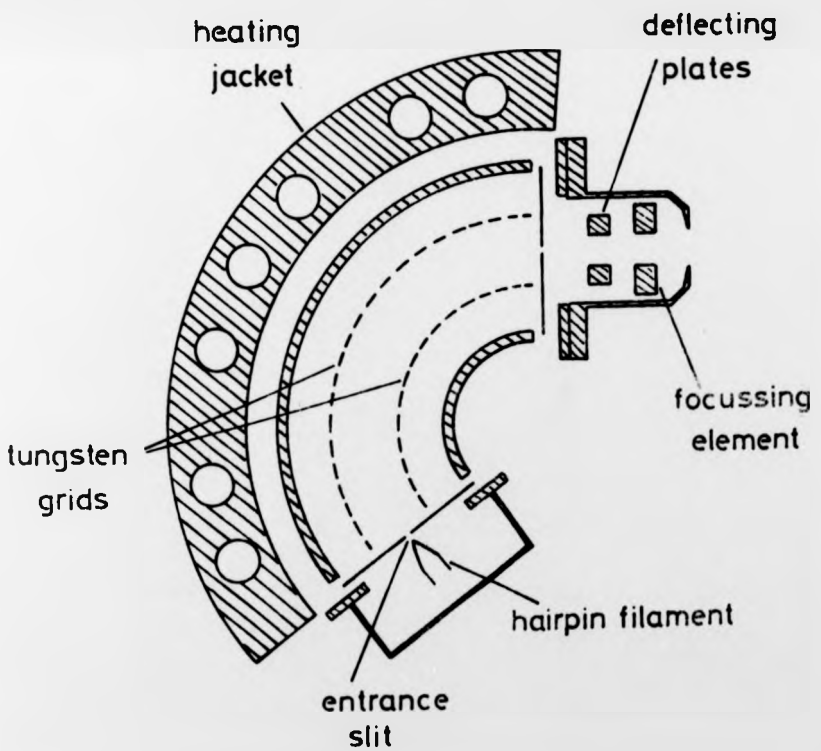

8:1 Sketch of the electron monochromator. Scale approximately 2:1

other by glass spacers and boron nitride insulators. The entrance and exit slits were made from molybdenum and were 0·4 mm wide, and 12·0 mm high. The cathode was a length of thoriated tungsten wire, bent into a hairpin, and placed about 0·6 mm behind the entrance slit. The cylindrical electrodes were made from 86·5% transparent tungsten gauze. These were spot-welded to copper frames. The technique for this was to first take a strand of silver-plated copper wire, and lightly tack this to the edge of the copper frame, using a fairly low current setting. Then, using this as a sandwich, the tungsten gauze was spotwelded on with tungsten electrodes, using a slightly higher current setting. A firm positive weld was obtained[45].

These transparent electrodes had solid cylindrical electrodes behind them, which were held at + 40 V to collect any electrons which passed through the gauzes. The two curved grids formed a channel 6·0 mm across and 23·0 mm high.

After the exit slit were a pair of beam-steering electrodes, which, taken together with a focussing electrode and the final aperture of the monochromator, formed a lens. 20 - 30V was normally applied to the focussing electrode to maximise the current reaching the Faraday cup. Each voltage applied to the monochromator came from an independent power supply.

The monochromator was mounted on a turntable with its axis perpendicular to the electron beam direction, so that it could be rotated about the axis of the detection optics. This facility proved valuable for making checks on the measured polarisation (see p.72).

The resolution of the monochromator is given approximately by

$$\frac{\Delta V_{\frac{1}{2}}}{V} = \frac{\Delta R}{R} + \frac{4}{3}\alpha^2$$

where $\Delta V_{\frac{1}{2}}$ is the resolution FWHM, V is the electron energy in the selector region, ΔR is the slit width, R is the mean radius of the cylindrical electrodes, and α is the divergence of the electrons at the entrance slit.

V was varied by altering the voltages applied to the inner and outer cylindrical gauze electrodes, and the energy resolution was measured by observing the resonance which appears at 4·92 eV in the 2537 A line. The half-width of this resonance was assumed to be much less than 100 meV, and so the measured half-width when the electron energy was scanned over this resonance, was just the resolution of the monochromator.

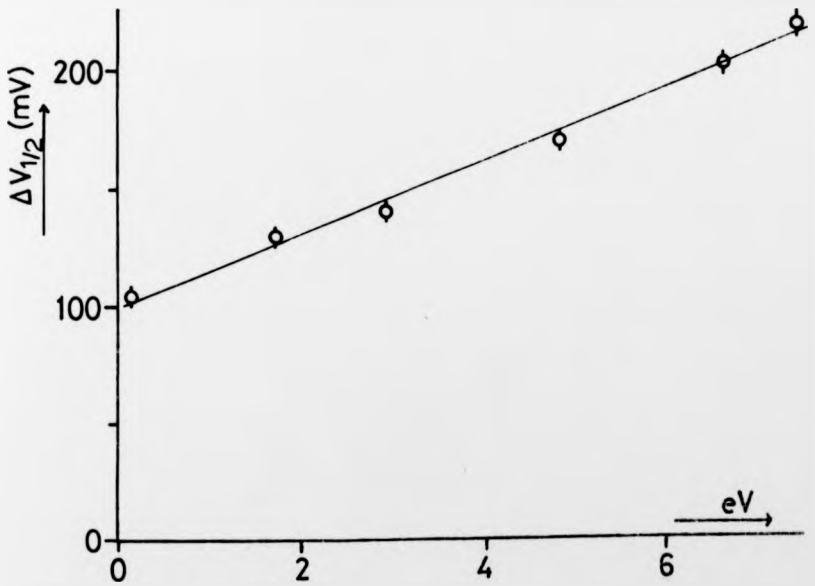

8:2 Energy resolution of the monochromator as a function of the energy of the electrons when traversing the selector region. Error bars indicate 90% confidence limits.

Fig. 8:2 shows $\Delta V_{\frac{1}{2}}$ plotted as a function of V. The points lie nearly on a straight line. The energy scale might be subject to a small shift, due to the effects of contact potential.

Fig. 8:3 shows $\Delta V_{\frac{1}{2}}$ plotted as a function of the transmitted current, and it can be seen that the current falls rapidly with decreasing instrumental half-width.

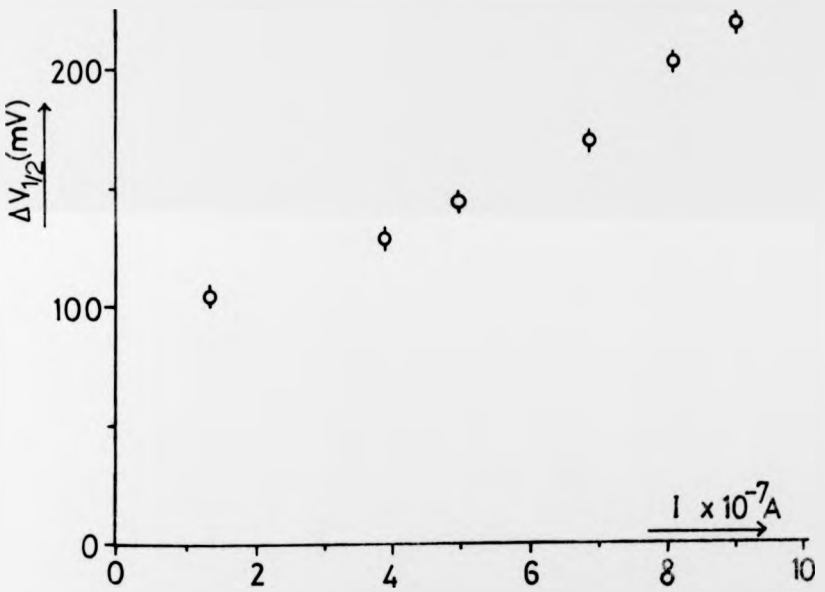

8:3 Resolution of the monochromator as a function of transmitted current. Error bars indicate 90% confidence limits.

After obtaining polarisation data for 100 meV resolution, the exit slit was reduced to 0·3 mm, and it was found that the resolution could be improved to 70 meV, with a transmitted current of about 8×10^{-8}A. The polarisation was not measured with this resolution

however.

The electrons left the monochromator at an energy of about 4·4 eV, and were accelerated slightly to the final energy of 4·5 - 8 eV, which was maintained over a field-free interaction region. The electrons were collected in a simple Faraday cup.

The monochromator was continuously baked at a temperature of 160°C. A jacket surrounding the instrument was heated by several ceramic rods wound with Kanthal wire in a bifilar way to eliminate magnetic fields. There was presumably a small residual field though, because there was a 4% increase in the electron current when the heating current was switched on. The effect of baking was to give great stability to the electron current and the resolution. Occasional shifts in the electron energy of up to 10 meV still occurred, but these were much worse without baking.

8.3 Optics

The optics used were similar to those used for the 1850 A line measurements, but the Rochon polariser was replaced with the Glan - Taylor polariser as was used in the vapour experiment. This allowed a larger interaction region to be visible, as there were no problems with both rays being transmitted. The spectrometer was replaced with a 1st order interference filter (see p. 27). Allowance had to be made for the change in focal length of the lenses with wavelength. Nitrogen flushing was no longer required, since the absorption of the 2537 A line by oxygen is negligible.

8.4 Electronics

A multichannel scaler (Intertechnique) was used for the collection of data for this measurement. The parallel output from the address register was fed into a digital to analogue converter (DAC), so that

as the channel number was repeatedly incremented, a voltage ramp was produced by the DAC. This voltage ramp was offset by a bias supply, and applied between the monochromator and the interaction region, so that the electron energy was scanned synchronously with the channel advance of the multichannel scaler. The photomultiplier pulses were fed into the multichannel scaling input via an amplifier and discriminator. The dwell time used was usually 1 ms/channel, and the DAC provided a voltage step of 19·3 mV or 25·6 mV /channel. Typically, 200 channels were scanned over repeatedly, so that a voltage range of 4 - 5 V was swept in 200 ms. A run consisted of up to 60000 sweeps with the polariser set to transmit $I_{\parallel}$, followed by the same number of sweeps for $I_{\perp}$. The method of obtaining the polarisation from the two excitation functions obtained by this method is described in the next section, along with the careful checks necessary.

9. Results from the High - resolution Experiment

9.1 Results

As described in the last section, the two excitation functions $I_{//}$ and $I_{\perp}$ were obtained separately, and the polarisation computed from them. The reason for employing this technique was to ensure that no unexpected shifts in voltage or changes in resolution occurred during a measurement; such changes showed readily on the multichannel scaler as an asymmetric shape to a resonance, or an apparent broadening of a resonance. Such effects usually completely disappeared after the monochromator had been operating for 4 - 5 hours. Typically, the energy range scanned through was from 4·6 eV onwards , so that the first 15 or so channels showed the background noise level. Because the two functions were obtained separately, there existed the possibility that the atomic beam density might have changed during the measurement of one of them, so that a procedure of normalisation was necessary. For this, the polarisation was measured accurately at one energy (5·50 eV) by repeatedly counting $I_{//}$ followed by $I_{\perp}$ each for 100 s. The polarisation was calculated from the averages. All the calculations were made on an ICL 4130 computer, the sequence of operations being listed below.

1. Data was output from the multichannel scaler to a teletype and paper-tape punch.

2. The paper tape was used as an input to the computer program.

3. The noise levels were found by averaging the first six channels each of $I_{//}$ and $I_{\perp}$, giving $D_{//}$ and $D_{\perp}$.

4. $(I_{//} - D_{//})$ and $(I_{\perp} - D_{\perp})$ were found for every channel.

5. The maximum of the resonance at 5·50 eV was located

9:1 Polarisation of the 2537 A line as a function of electron energy. Resolution = 140 meV. Error bars indicate 90% confidence limits, plus a small uncertainty in the systematic correction. The open circles are the calibration points discussed on p. 68 .

in both functions, and if not in corresponding channels, then $I_{//}$ was shifted along the energy scale the required number of channels to bring the maxima into coincidence. At most, this was 1 channel in either direction.

6. The ratio $g = (I_{//} - D_{//})/(I_{\perp} - D_{\perp})$ was found for each channel, and if the value was not the same at 5·50 eV as the accurately determined value (see above), then the ratio, g, was scaled up or down by the required amount, thus normalising the polarisations.

7. The polarisations were found from the relation $P = (g - 1)/(g + 1)$.

Further correction to the polarisation values was then made, because of the various instrumental effects described in section 9.2.

Fig. 9:1 shows the polarisation as measured with a resolution of 140 meV, together with several calibration points - the one at 5·50 eV mentioned above, and some more made in the same way. All the points lie well on the curve, thus indicating that the normalisation method is reliable.

Fig. 9:2 shows $I_{//}$, $I_{\perp}$ and the polarisation, P, for a resolution of 100 meV. The polarisation data are the average of four runs. The energy scale was calibrated by the threshold energy for the line (4·888 eV). The leading edge of the first resonance shows no serious departure from a Gaussian distribution shape, and it is deduced from this that the threshold for excitation lies within a few channels of the peak of the resonance.

In figs. 9:1 and 9:2, the error bars marked are 90% confidence limits for the statistical error, plus a small uncertainty in the

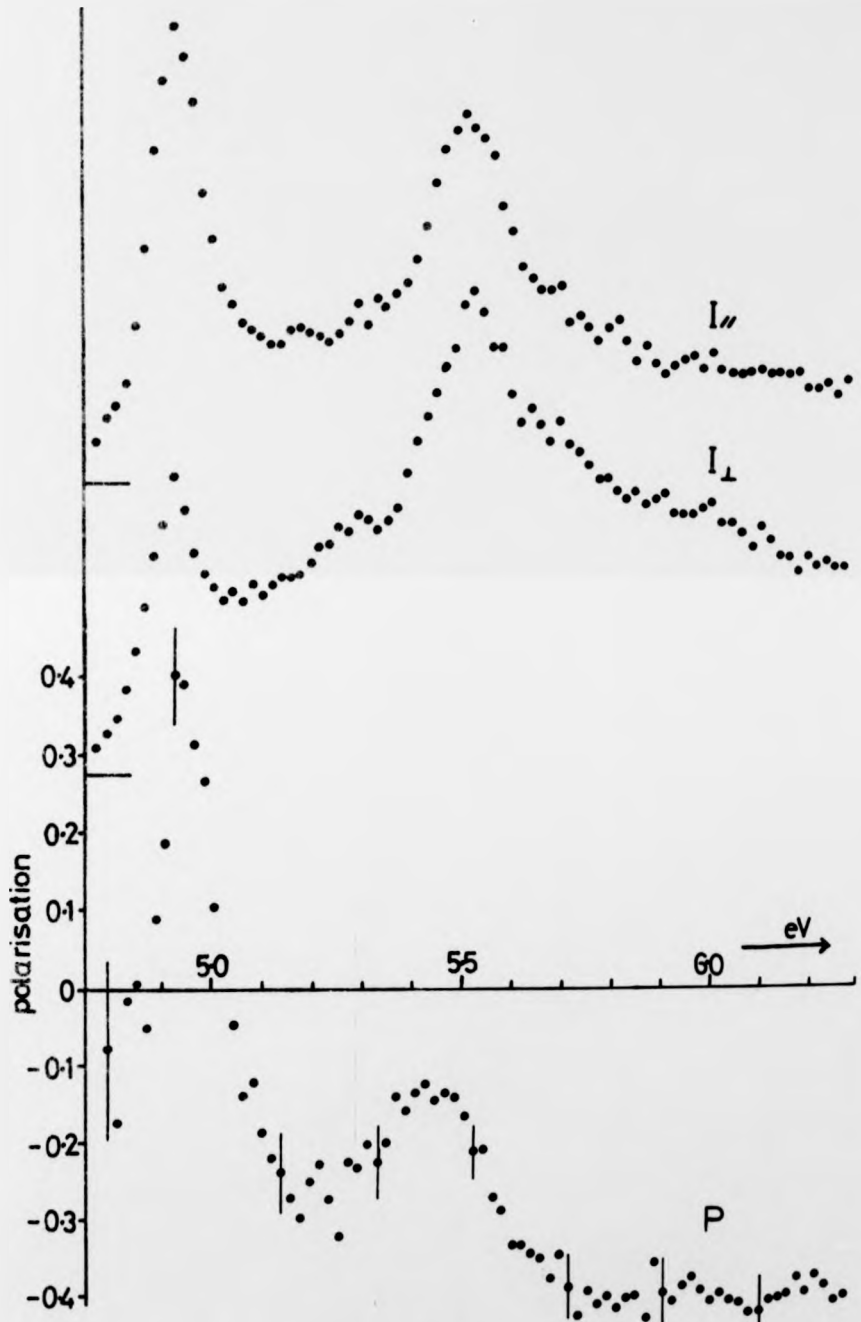

9:2 $I_{//}$, $I_{\perp}$, and polarisation, P , of the 2537 A line as a function of electron energy. Resolution = 100 meV. The top two curves are 'typical data' from a single run. The polarisation curve is the average of data derived from 4 sets of $I_{//}$ and $I_{\perp}$. Error bars are 90% confidence limits plus a small uncertainty in the systematic correction.

systematic correction which varied with the polarisation. This uncertainty was never greater than $\pm$ 0·03.

9.2 Sources of Error and Corrections

The same sources of error as listed in section 5.2 were again considered.

9.2.1 Pressure Depolarisation

With the mercury beam running, and the beam collector cooled to liquid nitrogen temperature, the pressure in the interaction region as measured by an ionisation gauge placed well away from the beam region was 2 x 10^{-6} Torr. As described in section 7.2.1, if the

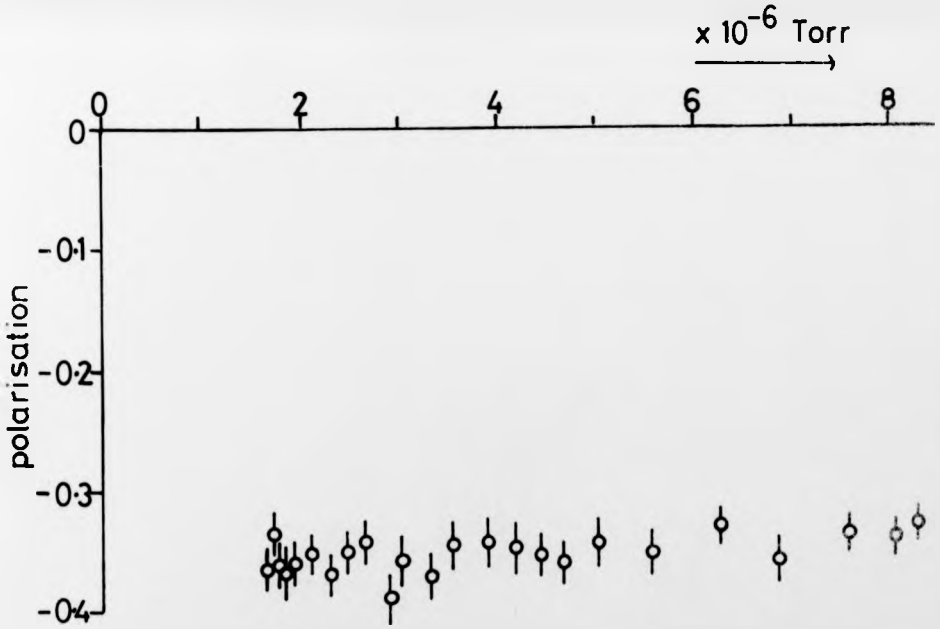

9:3 Pressure depolarisation of the 2537 A line in the crossed beam experiment. Error bars indicate 90% confidence limits.

collector plate was allowed to warm up, the mercury vapour pressure slowly rose into the 10^{-5} Torr range. The polarisation was measured at a fixed electron energy of 6·0 eV, as a function of mercury vapour pressure. The result is illustrated in fig. 9:3.

A linear extrapolation to zero pressure indicates a depolarisation at 2×10^{-6} Torr of 0·01, but this method is not accurate, and so a residual uncertainty of ± 0·01 was accepted, and included in the estimation of the error. In fact, this uncertainty was added to the statistical error, because it is not a constant systematic shift, but is a function of polarisation.

This method indicates the amount of depolarisation in the region between the beam and the window (a distance of 65 mm). The amount of depolarisation in the beam itself may be estimated in the following manner. The diameter of the mercury beam in the interaction region was estimated to be 6 mm, and the pressure to be 4×10^{-5} Torr. Thus the quantity (pressure x distance) was approximately the same for 2537 A photons travelling from the centre of the mercury beam to the edge of the beam, as for the photons travelling from the edge of the beam to the window (collecting lens). Thus the amount of pressure depolarisation in the two regions could be expected to be approximately equal, and the total pressure depolarisation correction applied to the data was 0·02 ± 0·02.

9.2.2 Instrumental Polarisation

As described in section 5.2.2, an instrumental polarisation of π results in a measured polarisation, P', being different to the true polarisation, P.

$$P' = \frac{\pi + P}{1 + \pi P}$$

Now suppose that the electron beam direction is rotated through

an angle δ about an axis running along the direction in which the radiation is observed, so that

$$I_{//} = I_z \cos^2\delta + I_x \sin^2\delta$$

and $$I_{\perp} = I_x \cos^2\delta + I_z \sin^2\delta$$

Then the apparent polarisation P_a (not the measured polarisation, P', which will have to take into account the instrumental polarisation, π) is given by

$$P_a = \frac{I_{//} - I_{\perp}}{I_{//} + I_{\perp}}$$

$$= \frac{(I_z - I_x)(\cos^2\delta - \sin^2\delta)}{(I_z + I_x)(\cos^2\delta + \sin^2\delta)}$$

$$= P \cos 2\delta \quad .$$

Thus, $$P' = \frac{P \cos 2\delta + \pi}{1 + P\pi \cos 2\delta} \quad .$$

For small π, this approximates to

$$P' = P \cos 2\delta + \pi \quad .$$

This equation suggested a method for determining the instrumental polarisation. P' was measured for several different values of δ, the result being shown in fig. 9:4. A total range in δ of about 50° was possible. Note that the curve is a typical $\cos 2\delta$ function. When first tried, however, the curve was offset by 7° from the assumed zero. This was unexpected, and was attributed to a deflection of the electron beam in the output stage of the monochromator, together with a possible misorientation of the polariser. To overcome this problem, the electron gun was thereafter set 7° away from the previous $\delta = 0$ position, and a repeat of the above experiment (i.e. P' as a function of δ) gave a $\cos 2\delta$ curve centred on $\delta = 0$, as it should.

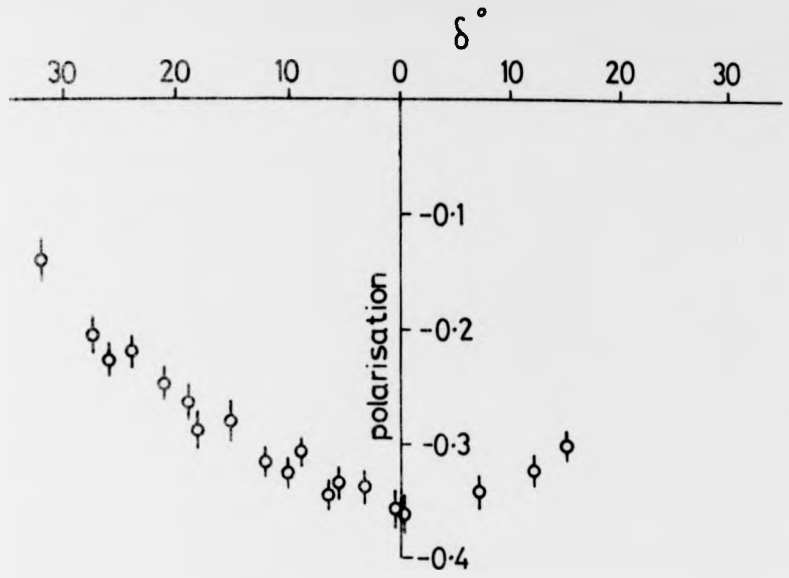

9·4 Polarisation of the 2537 A line as a function of δ (explained in text). Electron energy 6·5 eV. Error bars represent $\pm$ 1 standard deviation.

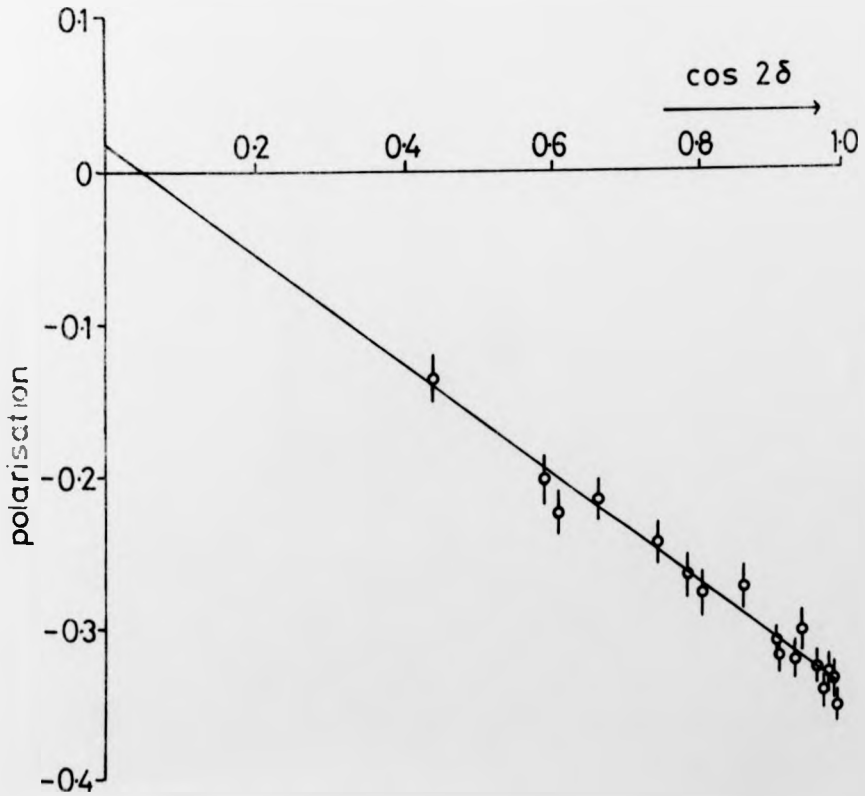

9:5 Polarisation data from fig. 9:4, replotted as a function of cos 2δ . The straight line is a least squares fit.

To find the value of π, P' was plotted against cos 2δ (fig. 9:5), and the intercept found on the ordinate axis by making a least squares fit of the data points to a straight line. This procedure gave $\pi = 0{\cdot}017 \pm 0{\cdot}014$.

9.2.3 Divergence of the Electron Beam

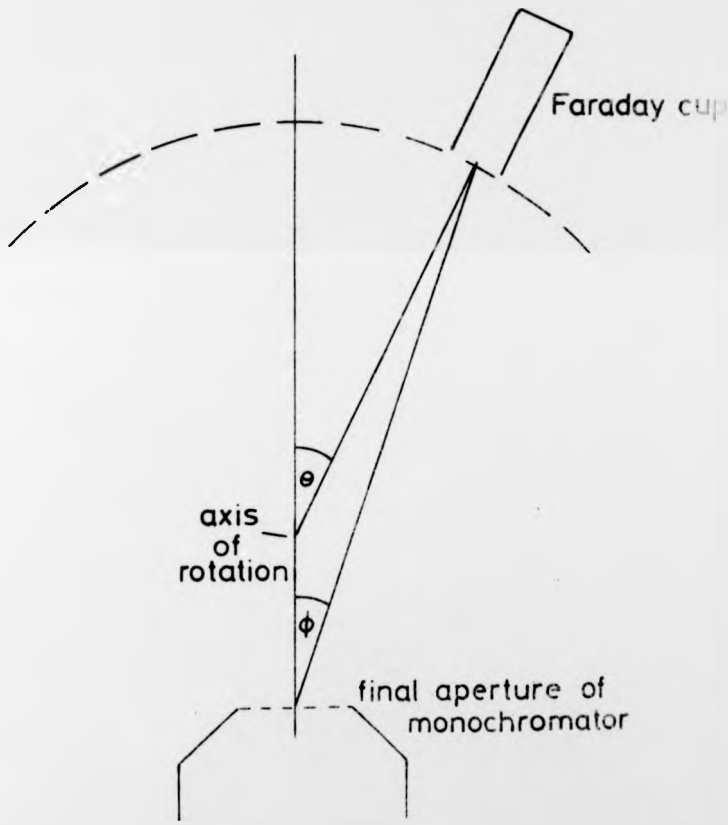

9:6 Experimental arrangement used for measuring the electron beam divergence.

This was measured by removing the usual Faraday cup, and replacing it with a much smaller one, 4·0 mm in diameter, placed a distance of 40 mm away from the final aperture of the monochromator. It was not fixed to the turntable, however, so that the electron beam could be scanned across it, by rotating the turntable holding the monochromator. The geometry of the arrangement is shown in fig. 9:6. The aperture marked is the longest dimension of the final aperture (8 x 4 mm). The beam divergence could not be measured in the plane perpendicular to this, and had to be assumed to be essentially similar. Θ is the measured angle through which the monochromator was rotated, and it had to be related to ϕ , the divergence angle of the electron beam.

Fig. 9:7 shows the current collected by the Faraday cup as a function of ϕ . Note that the shape is somewhat asymmetric. The angular width of the distribution (FWHM) is about 15°, but account must be taken of the angular width of the Faraday cup ($\sim 5^{\circ}$), and when this is done, the width reduces to approximately 12°. The polarisation data were corrected according to the equation given in section 5.2.3. An approximation made in the above method was to assume that electrons emerged from only a small region in the centre of the aperture.

9.2.4 Other Sources of Error

The polarisation values were corrected for the effect of finite solid angle of photon detection (see section 5.2.4).

Helmholtz coils were used to cancel the earth's magnetic field in the interaction region. The residual magnetic field was measured to be less than 10 mG over a 1000 cm^3 volume, centred on the interaction region. No correction to the polarisation data was made for this small field.

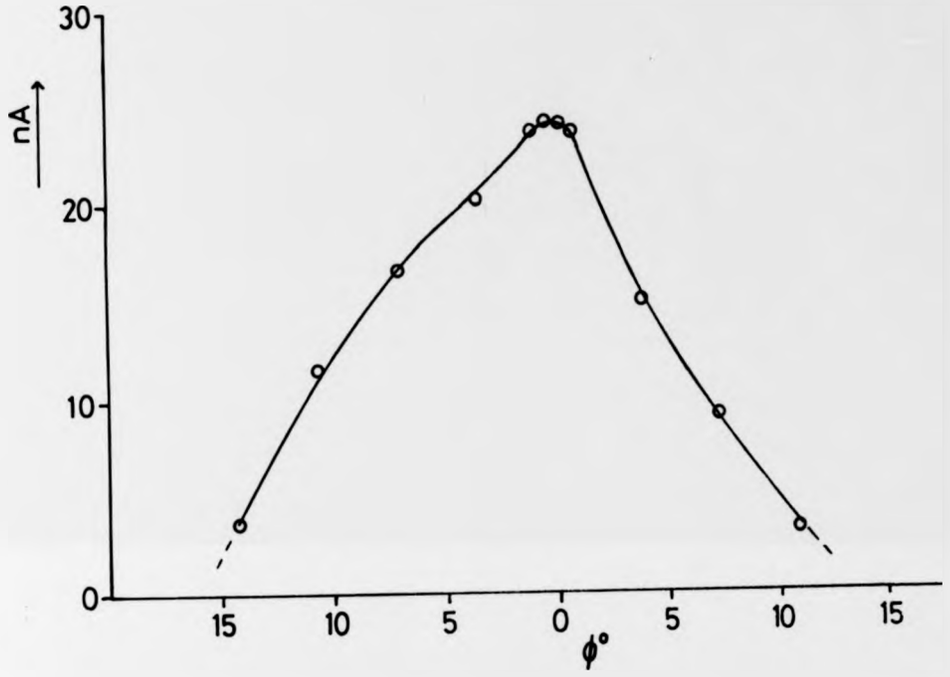

9:7 Divergence of the electron beam. The current collected by the Faraday cup has been plotted as a function of the angle ϕ (see fig. 9:6).

10. Discussion of the Results

10.1 The 1850 A Line

Fig. 10:1 illustrates a comparison of the results obtained (see section 7) with the theory of McConnell and Moiseiwitsch[28]. The units along the abcissa are $(V/V_o)^{\frac{1}{2}}$, where V_o is the excitation threshold energy (6·70 eV). It will be seen that above about 1·2 (9·4 eV), there is a good agreement between theory and experiment, particularly if the measured values are shifted upwards by the estimated systematic error of 0·04. Below 1·15 (8·8 eV), however, there is a marked disagreement, and the polarisation drops steadily towards threshold. It must be stressed that this in no way implies that the threshold polarisation will be very small, since the polarisation could not be measured below 7·0 eV, and in any case, the energy resolution would not permit sudden changes in polarisation near threshold to be observed.

It may well be possible that there are unresolved resonances in the region just above threshold, which are affecting the polarisation in the observed manner. This is seen to be the case for the 2537 A line. The dip in the polarisation centred around 1·22 (10·0 eV) may also be caused by a resonance.

It should be noted that cascading may affect this line above 7·7 eV (populating the upper 6^1P_1 level by transitions from the 7^3S_1 level), although this is possibly not serious, since, as Penney[9] has discussed, direct excitation of the 6^1P_1 level is likely to dominate over any cascade processes. However, Jongerius[46] took the opposite view. Indeed, it is possible that it is the cascading which reduces the polarisation at low energies, and that the theoretical value is only reached when the direct excitation of the 6^1P_1 level has grown

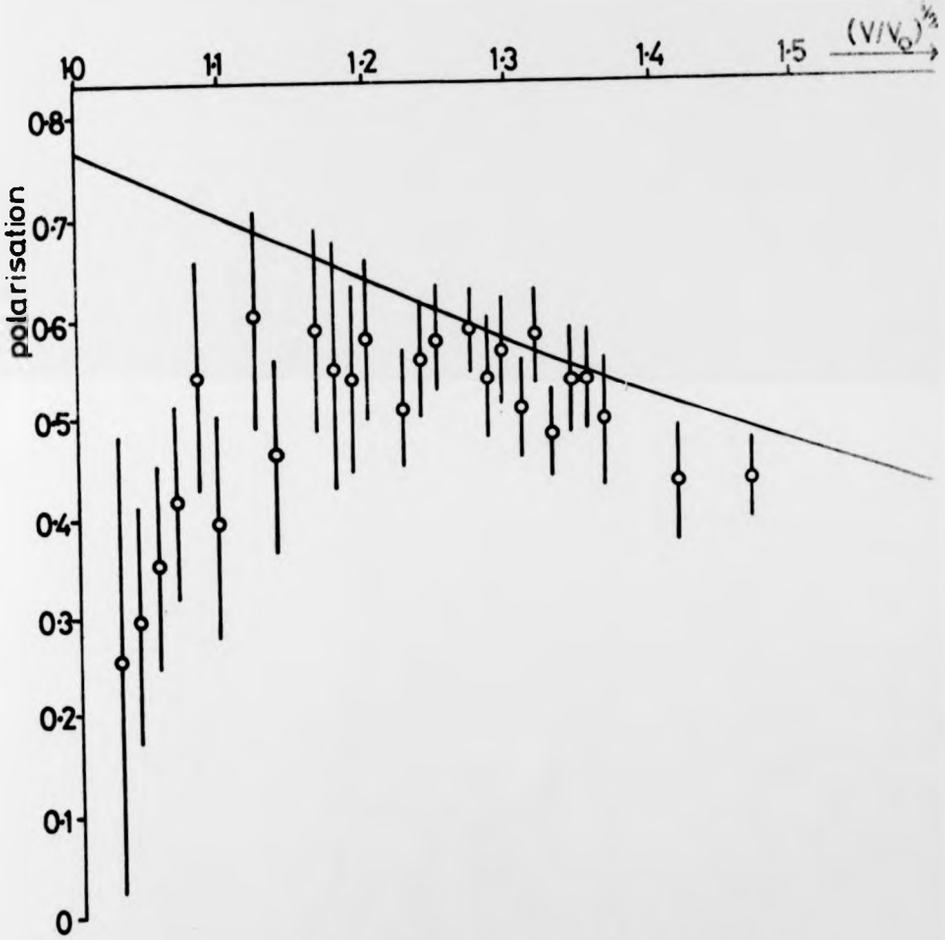

10:1 Comparison of the theory of McConnell and Moiseiwitsch (solid curve) with the measured values for the 1850 A line. Abcissa units are $(V/V_o)^{\frac{1}{2}}$, where V_o is the threshold energy. The plotted points are the same as shown in fig. 7:1.

large compared with cascade processes. If this explanation were correct, it would follow that below 7·7 eV, the theoretical polarisation would again be reached. The data obtained in the present experiment are not sufficiently precise in this region to be able to say whether this suggestion is correct or not.

10.2 The 2537 A Line

The upper part of fig. 10:2 shows $\bar{I}$, as defined in equation (3 - 5), that is, $\bar{I} = \frac{2}{3}(I_{//} + 2\,I_{\perp})$. The lower part shows the measured polarisation, and the theoretical curve of McConnell and Moiseiwitsch, as well as the experimental results of Skinner and Appleyard[6]. The data were taken with an energy resolution of 140 meV. It can be seen that the polarisation of this line is dominated at low energies by the presence of the resonances at 4·92 and 5·50 eV (for the calibration of the energy scale, see section 10.3.2). Also, above about 8·0 eV, there are more resonances, and a strong indication in the $\bar{I}$ curve that cascading is important for this line.

Nevertheless, in the region 6·2 - 7·9 eV, the polarisation varies smoothly with energy, and may be compared with the theory. It is clear that although the agreement is generally good, the slopes of the two curves in this region are different, so that while at 6·2 eV the agreement is nearly perfect, at 7·7 eV there is a discrepancy of 0·05 in the polarisation.

From the results of the vapour experiment, it appeared as if the sudden increase in polarisation just above threshold, approaching from higher energies, was an indication of a large negative threshold

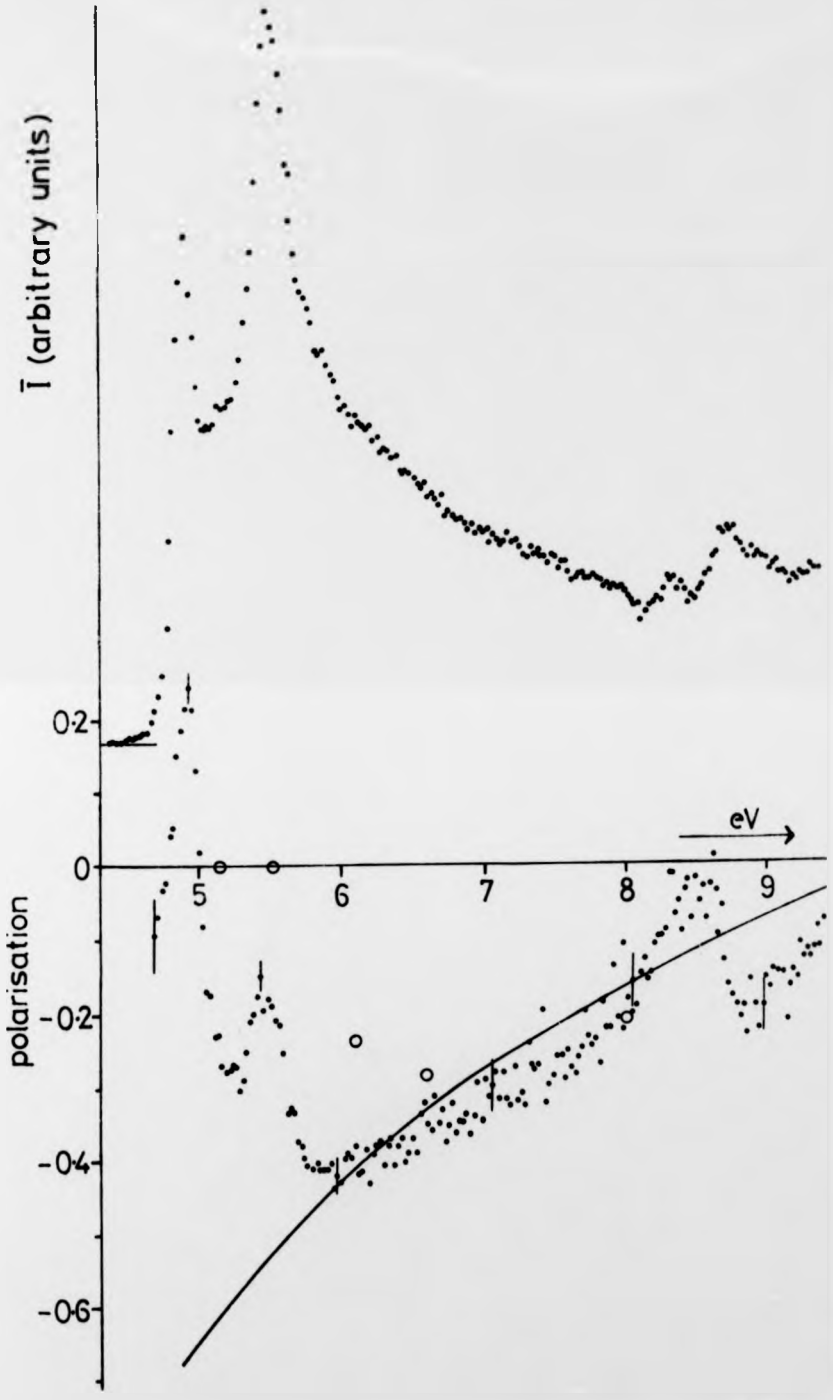

10:2 $\bar{I}$ (upper) and polarisation (lower) of the 2537 A line, for an energy resolution of 140 meV. Error bars indicate 90% confidence limits, plus a small uncertainty in the systematic correction. The solid line is the theory of McConnell and Moiseiwitsch; the circles are the data of Skinner and Appleyard.

polarisation. Furthermore, it was expected that an improvement in resolution would show the effect more clearly. However, the FWHM of the energy spread was reduced from about 300 meV to 200meV, and then to 100 meV, and although the height of the resonance just above threshold increased dramatically, the value of the polarisation for the 'first measurable point' remained essentially unaltered at between - 0·10 and - 0·20. From this it may be deduced that the drop in polarisation occurs very close indeed to threshold, and that the actual threshold polarisation is probably not measurable in this type of experiment (but see Imhof and Read[47] for a coincidence method, applied to helium by King, Adams and Read[48], and to be extended to mercury).

It should be noted that Chow Chiu[49] has considered the possibility of a magnetic interaction occurring between the spin of the outgoing electron and the angular momentum of the atom, leading to a disorientation of the atom, and a subsequent reduction in the polarisation at threshold.

It is interesting to compare the data from the vapour experiment with those from the high resolution experiment. The two sets of results should be directly comparable, apart from the difference in energy resolution. Fig. 10:3 shows the comparison. Both sets have been plotted together, but the earlier results had to be shifted downwards in energy by 0·2 eV in order to get the best agreement. This implies that the original energy scale calibration was wrong for the vapour experiment. The method of calibration, as stated on p.31 , was to set the main peak of excitation at 5·6 eV, this value being taken from the work of Zapesochnyi and Shpenik[33]. However, as discussed in section 10.4.1, this energy is probably

more nearly 5·5 eV. This accounts for half the necessary shift. The origin of the remaining shift is unknown. Otherwise, the agreement is adequate, apart from a tendency above about 7 eV for the polarisation as measured in the vapour experiment to be consistently more negative than in the other set of data.

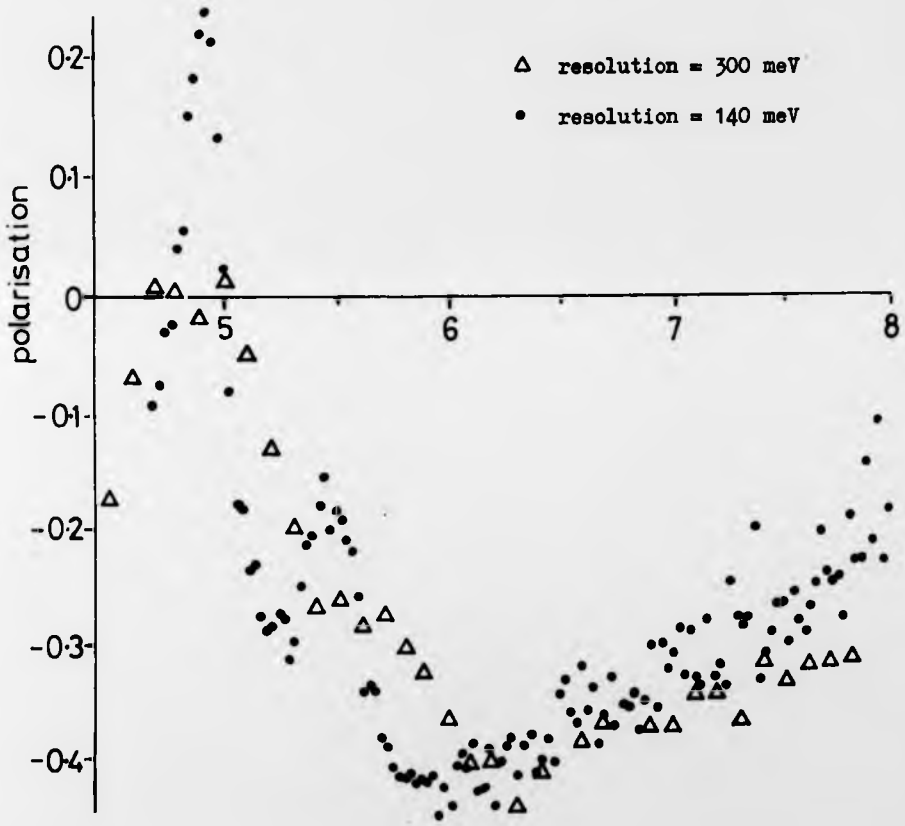

10:3 Comparison of the results from the vapour experiment (resolution 300 meV), with the results from the high resolution experiment (resolution = 140 meV). The energy scale of the vapour experiment results has been shifted by 0·2 eV to give a better fit.

10.3 Calibration of the Energy Scale

10.3.1 The 1850 A Line

The method of calibrating the energy scale is described in section 7.1. It was necessary to be quite certain of the threshold energy of this line, because Jongerius[46] found that the threshold was not coincident with the 6^1P_1 level, but occurred 1·2 eV higher at the position of the 7^3S_1 level (7·9 eV). This surprising result came from comparing the apparent threshold of the 1850 A line with thresholds of other measured lines - those at 5461, 4078 and 5790 A, and assuming the threshold energies of these lines to be just the spectroscopic values. The detection sensitivity of that experiment was probably not as great as in the present experiment, and this fact probably explains the discrepancy, particularly when the rather shallow onset of excitation of the line is taken into account (see fig. 7:1)

The shape of the excitation function as measured here, agrees fairly well with that found by Jongerius. Shregardus[50], who also measured this excitation function, found a different sort of shape altogether, with a large broad peak in the cross-section just above threshold, which it would have been impossible in the present experiment to have overlooked. The method Shregardus used for isolating the line was to record the photon signal alternately with, and without, oxygen absorbing the 1850 A line, and then to find the difference in signal. This method would appear to be insufficiently reliable.

In the region 10 - 11 eV, the energy scale is probably not linear, due to space-charge depression below ionisation threshold, and a neutralisation of this effect above ionisation threshold.

10.3.2 The 2537 A Line

As fig. 10:2 shows, the onset of excitation for this line is

extremely steep, due to the presence of the resonance. This onset was examined many times, with varying resolution, and in every case, the shape of the leading edge of the resonance was just that of the energy spread of the electron beam (assumed to be Gaussian). In other words, there was no sign of any excitation below the resonance, from which it was deduced that the resonance centre was only very slightly above threshold. The smallest FWHM of energy spread used to examine the threshold region was 70 meV, so that from where the excitation first appeared out of the noise, to the peak of the resonance was also approximately 70 meV.

It was thought reasonable therefore to place the threshold about half way up this slope, i.e. 30 meV below the peak of the resonance, but with an error of 30 meV, so as to include the possibility that the resonance is actually centred on threshold. So that, since the spectroscopic threshold energy is 4·888 eV, the resonance position was placed at 4·92 ± 0·03 eV.

This calibration then fixed the positions of the other resonances occurring in the excitation of the line. The assumption was made that there was no space-charge effect causing a non-linearity in the energy scale. This assumption was justified on the grounds that since the monochromator was probably operating in a space-charge limited mode, then in any elements after the exit slit, where the voltages were higher and the apertures larger, the electron beam should no longer be space-charge limited, and that space-charge depression should then only be a small effect.

10.4 Discussion of the Resonances in the 2537 A Line

10.4.1 Positions of the Resonances

Following on from the last sub-section, table 10:1 lists the

measured positions of all resonances and similar features observed either in $I_{//}$, $I_{\perp}$ or both. It is recognised that not all of these features may be due to the formation of excited states of the negative ion, Hg^-.

Table 10:1

Position of observed feature	Observed in:
4·92 eV	$I_{//}$, $I_{\perp}$
5·23	$I_{\perp}$
5·50	$I_{//}$, $I_{\perp}$
8·38	$I_{//}$, $I_{\perp}$
8·76	$I_{//}$, $I_{\perp}$
9·04	$I_{//}$

In each case the positional uncertainty is ± 0·03 eV.

Of these, the three resonances at 8·38, 8·76 and 9·04 eV are all above the threshold for cascading from the 7^3S_1 level, via the 4358 A line to the 6^3P_1 level. It is not possible to say from the present work whether these resonances are in the direct excitation of the 6^3P_1 level, or in the excitation of the 7^3S_1 level. Other workers, however, have observed similar structure in the excitation of the 7^3S_1 level, by measuring the excitation function of any of the three lines $6^3P_{0,1,2} - 7^3S_1$. Thus Zapesochnyi and Shpenik[33] observe a resonance in the 5461 A line at 8·8 eV, and Smit and Fijnaut[51] apparently observe the same feature at about 8·5 eV.

Zapesochnyi and Shpenik[33] also observed resonances in the excitation function of the 2537 A line. Table 10:2 compares the positions given by those authors with the positions found in the present work. The agreement is very good, apart from an overall shift in energy of about 0·1 eV.

Table 10:2

Zapesochnyi and Shpenik	Present work
5·0 eV	4·92 eV
5·3	5·23
5·6	5·50
8·5	8·38
9·0	8·76

Less good, however, is the agreement with the electron transmission data of Kuyatt, Simpson and Mielczarek[52]. It has been suggested by Burrow and Michejda[53] that an energy scale calibration error might be responsible for the discrepancy between the results of Kuyatt et al and their own results from essentially the same type of experiment. Burrow and Michejda have observed resonances in the transmission of electrons at the positions given in table 10:3, which also lists the positions found by Kuyatt et al.

Table 10:3

Burrow and Michejda	Kuyatt et al
4·68 eV	4·07 eV
4·91	4·29
5·50	4·89

Of these, only the last two should be observable in the 2537 A line, since the other is below threshold. This is indeed the case, and the agreement of the results of the present experiment with those of Burrow and Michejda is excellent. The small feature observed in the present work at 5·23 eV was not seen by Burrow and Michejda. The widths of the resonances are also worth comparing. As described in section 8.2, the width of the resonance at 4.92 eV was assumed to be much less than the instrumental half-width, and was used as a measure of the energy resolution of the monochromator. The smallest width (FWHM) measured for this resonance was 70 meV, and thus the actual width will be certainly smaller than this. For the 5·50 eV

resonance, the measured FWHM was about 140 meV, and since the instrumental resolution was then less than 70 meV, the actual width of this resonance would be approximately 120 meV (the half-widths add in quadrature). The widths found for the two resonances by Burrow and Michejda are ~40 meV and ~115 meV respectively.

It is therefore almost completely certain that the resonances observed by Burrow and Michejda at 4·91 and 5·50 eV are the same features as are observed in the present experiment at 4·92 and 5·50 eV.

In an electron scattering experiment, Duweke, Kirchner, Reichert and Staudt[54] determined the positions of the same two resonances to be 4·55 ± 0·10, and 5·15 ± 0·10 eV. Their calibration of the energy scale was done using a gas mixture of mercury and nitrogen, and finding the nitrogen resonance at 1·87 eV. It is not clear why these discrepancies in the resonance positions should arise.

10.4.2 Identification of the Resonances

Following the results of Kuyatt, Simpson and Mielczarek[52], Fano and Cooper[55] put forward a possible identification of the negative ion states being formed. Their identifications are listed in table 10:4.

Table 10:4

Position of resonance (from Kuyatt et al)	Negative ion state (from Fano and Cooper)
4·07 eV	$6s6p^2\ {}^4P_{1/2}$
4·29	$6s6p^2\ {}^4P_{3/2}$
4·89	$6s6p^2\ {}^4P_{5/2}$

The 'parent' levels of these negative ion states are the $6s6p\ {}^3P_{0,1,2}$ levels of the neutral atom. The addition of a second electron into the 6p subshell would not be expected to change the energy of the level to any great extent, and this is partly the basis of the identification by Fano and Cooper. If however, the

results of Kuyatt et al were subject to a miscalibration of the energy scale as Burrow and Michejda suggest, then this places the $^4P_{3/2}$ state at 4·92 eV and the $^4P_{5/2}$ state at 5·50 eV.

In the case of the 4·92 eV resonance, it is so close to the threshold of the 2537 A line, that the threshold selection rule $\Delta M_L = 0$ probably still applies, thus the formation of a negative ion state with a J value of other than 1/2 or 3/2 would be impossible. The present experiment provides a method of distinguishing between these two states. Baranger and Gerjuoy[21] have computed the theoretical polarisation of the emitted radiation for the two cases, and predict zero polarisation for a $P_{1/2}$ negative ion state, and + 0·60 for a $P_{3/2}$ state. This is not taking into account the effect of observing radiation from the normal mixture of isotopes, for which the expected polarisation would be less.

In the present experiment, the polarisation of the 4·92 eV resonance was found to increase as the FWHM of the energy spread in the incident electron beam was reduced. This is shown in table 10:5

Table 10:5

Energy resolution	Measured polarisation at peak of resonance at 4·92 eV
300 meV	0·00 ± 0·04
200	0·15 ± 0·04
140	0·24 ± 0·03
100	0·40 ± 0·07

The errors shown in the polarisation are 90% confidence limits, plus a small uncertainty in the systematic correction.

Thus, a further improvement in energy resolution could be expected to lead to a further increase in the polarisation of this resonance. It can be seen, therefore, that the hypothesis that the resonance at 4·92 eV is caused by the formation of a $^4P_{3/2}$ negative ion state

appears to be supported by the polarisation data.

The 5·50 eV resonance is too far above threshold for it still to be true that the inelastically scattered electron will remove no angular momentum from the system, and so it is quite possible for a J = 5/2 negative ion state to be observed in the excitation of the 6^3P_1 level. Unfortunately, no theoretical values for the polarisation of the emitted line radiation for this case are available, and so no further comparison can be made.

In the experiment of Duweke et al[54], mentioned on p.87 , it was found that the angular distribution of the scattered electrons supported the identification of these resonances as $^4P_{3/2}$ and $^4P_{5/2}$.

Appendix 1

Correction to Polarisation Measurements due to the Finite Convergence Angle of the Electron Beam

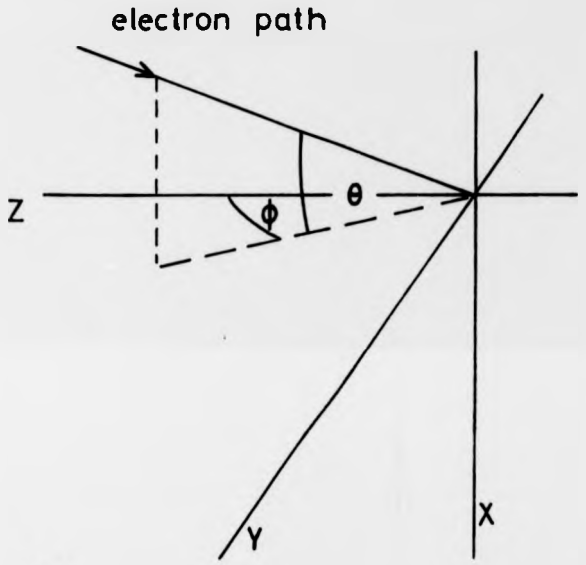

A:1

With reference to fig. A:1, the electron beam is nominally along the Z axis, and the emitted radiation is observed along the Y axis. The diagram shows an electron path which is inclined to the Z axis at an angle $(\theta^2 + \phi^2)^{\frac{1}{2}}$, this angle being resolved into two components ϕ and θ for ease of analysis. It is assumed that this angle has some (small) limiting value α, and that the distribution of electron paths is uniform within a cone of half - angle α.

If all the electron paths were along the Z axis (the ideal case), the measured polarisation would be given by

$$P = \frac{I_{//} - I_{\perp}}{I_{//} + I_{\perp}}$$

However, the divergence of the electron beam results in the measured $I'_{//}$ and $I'_{\perp}$ being different to $I_{//}$ and $I_{\perp}$.

$$I'_{//} = I_{//}\cos^2\theta\cos^2\phi + I_{\perp}\sin^2\theta\cos^2\phi + I_{\perp}\sin^2\phi$$

$$I'_{\perp} = I_{\perp}\cos^2\theta + I_{//}\sin^2\theta$$

Making the small angle approximation, $\sin x = x$, $\cos x = 1 - \frac{x^2}{2}$,

$$I'_{//} = I_{//}(1 - \theta^2 - \phi^2) + I_{\perp}(\theta^2 + \phi^2) ,$$

$$I'_{\perp} = I_{\perp}(1 - \theta^2) + I_{//}\phi^2 ,$$

neglecting terms of higher order than θ^2.

All the possible electron trajectories are now integrated over. If the trajectories are uniformly distributed within a cone, then the averages, $\bar{I}_{//}$ and $\bar{I}_{\perp}$ may be defined by,

$$\bar{I} = \frac{4}{\pi\alpha^2}\int_0^{\theta_{MAX}}\int_0^{\phi_{MAX}} I' \, d\phi \, d\theta ,$$

where $\theta_{MAX} = \alpha$,

and $\phi_{MAX} = (\alpha^2 - \theta^2)^{1/2}$

Solving these integrals (with the aid of a $\theta = \alpha\sin\psi$ substitution) gives the result

$$\bar{I}_{//} = I_{//}(1 - \frac{\alpha^2}{2}) + I_{\perp}\frac{\alpha^2}{2} ,$$

$$\bar{I}_{\perp} = I_{//}\frac{\alpha^2}{4} + I_{\perp}(1 - \frac{\alpha^2}{4}) .$$

P_m, the measure polarisation is now defined by

$$P_m = \frac{\bar{I}_{//} - \bar{I}_{\perp}}{\bar{I}_{//} + \bar{I}_{\perp}}$$

$$= \frac{P(1 - \frac{3}{4}\alpha^2)}{1 - P\frac{\alpha^2}{4}}$$

$$\therefore P = P_m / (1 - \frac{3\alpha^2}{4} + P_m\frac{\alpha^2}{4})$$

Appendix 2

Correction to Polarisation Measurements due to the Finite Solid Angle of Photon Detection

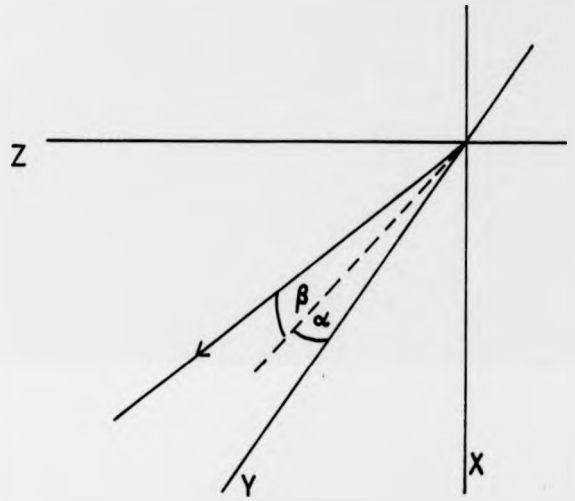

A:2

Refering to fig. A:2, the effect of detecting photons in a direction which is inclined to the Y axis is again a depolarisation. The diagram shows a direction inclined at an angle of $(\alpha^2 + \beta^2)^{\frac{1}{2}}$ to the Y axis, again resolved into two components, with α lying in the YZ plane. Applying a similar treatment to that used in Appendix 1,

$$I'_{//} = I_{//} \cos^2\alpha + I_{\perp} \sin^2\alpha$$

$$I'_{\perp} = I_{\perp} \cos^2\beta + I_{\perp} \cos^2\alpha \sin^2\beta \quad ,$$

and making the small angle approximation,

$$I'_{//} = I_{//}(1 - \alpha^2) + I_{\perp}\alpha^2$$

$$I'_{\perp} = I_{\perp}$$

Now suppose that photons may be detected anywhere over a circular aperture (e.g. a lens), which subtends a half - angle γ at the interaction region. Then the average intensities $\bar{I}_{//}$ and $\bar{I}_{\perp}$ detected will be given by

$$\bar{I} = \frac{4}{\pi\gamma^2}\int_0^{\beta_{max}}\int_0^{\alpha_{max}} I' \, d\alpha \, d\beta \quad ,$$

where $\beta_{max} = \gamma$

and $\alpha_{max} = (\gamma^2 - \beta^2)^{1/2}$.

Solving these integrals gives

$$\bar{I}_{//} = I_{//}\left(1 - \frac{\gamma^2}{4}\right) + I\frac{\gamma^2}{4} \quad ,$$

$$\bar{I}_{\perp} = I_{\perp} \quad ,$$

and hence $$P_m = \frac{P\left(1 - \frac{\gamma^2}{4}\right)}{1 - P\frac{\gamma^2}{4}}$$

$$\therefore \quad P = P_m / \left(1 - \frac{\gamma^2}{4} + P_m\frac{\gamma^2}{4}\right) .$$

References

1. W.Kossel and C.Gerthsen Ann. d. Physik, 77, 273 (1925).
2. A.Ellett, P.D.Foote and F.L.Mohler Phys. Rev., 27, 31 (1926).
3. H.W.B.Skinner Proc. Roy. Soc., A112, 642 (1926).
4. J.A.Eldridge and H.F.Olson Phys. Rev., 28, 1151 (1926).
5. von B.Quarder Z. f. Physik, 41, 674 (1927).
6. H.W.B.Skinner and E.T.S.Appleyard Proc. Roy. Soc., A117, 224 (1927).
7. J.R.Oppenheimer Z. f. Physik, 43, 27 (1927).
8. J.R.Oppenheimer Proc. Nat. Acad. Sci., 13, 800 (1927).
9. W.G.Penney Proc. Nat. Acad. Sci., 18, 231 (1932).
10. V.L.Federov and A.P.Mezentsev Opt. Spektrosk., 19, 12 (1965); Opt. Spectrosc., 19, 5 (1965).
11. H.G.M.Heideman, C.Smit and J.A.Smit Physica, 45, 305 (1969).
12. I.C.Percival and M.J.Seaton Phil. Trans. Roy. Soc., A251, 113 (1958).
13. R.H.McFarland Phys. Rev., 133A, 986 (1964).
14. D.W.O.Heddle and R.G.W.Keesing Proc. Roy. Soc., A299, 212 (1967).
15. D.W.O.Heddle, R.G.W.Keesing and R.D.Watkins Proc. Roy. Soc., A337, 443 (1974).
16. H.Hafner, H.Kleinpoppen and H.Kruger Phys. Letters, 18, 270 (1965).
17. E.A.Enemark, thesis, University of Colorado (1971).
18. V.J.Ehlers and A.C.Gallagher Phys. Rev., A7, 1573 (1973).
19. H.Kleinpoppen and E.Kraiss Phys. Rev. Lett., 20, 361 (1968).
20. W.R.Ott, W.E.Kauppila and W.L.Fite Phys. Rev. Lett., 19, 1361 (1967).
21. E.Baranger and E.Gerjuoy Proc. Phys. Soc., 72, 326 (1958).
22. D.H.Crandall, P.O.Taylor and G.H.Dunn unpublished, cited in ref. 27.
23. D.W.O.Heddle and R.G.W.Keesing in 'Advances in Atomic and Molecular Physics', vol. 4 , D.R.Bates and I.Estermann eds. (1968).
24. H.Kleinpoppen in 'Physics of the One- and Two-electron Atoms', F.Bopp and H.Kleinpoppen eds. (1969).
25. T.W.Ottley, D.R.Denne and H.Kleinpoppen Phys. Rev. Lett., 29, 1646 (1972).

26. T.W.Ottley, D.R.Denne and H.Kleinpoppen J.Phys.B, 7, L179 (1974).

27. U.Fano and J.H.Macek Rev. Mod. Phys., 45, 553 (1973).

28. J,C.McConnell and B.L.Moiseiwitsch J.Phys.B, 1, 406 (1968).

29. V.I.Ochkur Sov. Phys. JETP, 18, 503 (1964).

30. J.R.Pierce 'Theory and Design of Electron Beams', van Nostrand, 2nd edition (1954).

31. A.Lurio Phys. Rev., 140A, 1505 (1965).

32. B.L.Moiseiwitsch and S.J.Smith Rev. Mod. Phys., 40, 238 (1968).

33. I.P.Zapesochnyi and D.B.Shpenik Sov. Phys. JETP, 23, 592 (1966).

34. G.K.Woodgate 'Elementary Atomic Structure', McGraw-Hill, (1970).

35. J.N.Dodd, W.J.Sandle and O.M.Williams J. Phys. B, 3, 256 (1970).

36. A.C.G.Mitchell and M.W.Zemansky 'Resonance Radiation and Excited Atoms', Macmillan (1934).

37. J.A.Simpson and C.E.Kuyatt Rev. Sci. Instr., 34, 265 (1963).

38. I.Langmuir Phys. Rev., 21, 419 (1923).

39. K.R.Spanenberg 'Vacuum Tubes', McGraw-Hill (1948).

40. K.Watanabe, E.C.Y.Inn and M.Zelikoff J.Chem. Phys., 21, 1026 (1953).

41. A.Matsui and W.C.Walker J.Opt. Soc. Am., 60, 64 (1970).

42. E.Poulsen Appl. Optics, 11, 1876 (1972).

43. V.Raible thesis, University of Stirling (1974).

44. P.Marmet and L.Kerwin Can. J. Phys., 38, 787 (1960).

45. D.F.Dance and C.Duncan J.Phys. E, 5, 10 (1971).

46. H.M.Jongerius Philips Res. Rep. suppl. no. 2 (1961).

47. R.E.Imhof and F.H.Read J. Phys. B, 4, 450 (1971).

48. G.C.M.King, A.Adams and F.H.Read J. Phys. B, 5, L254 (1972).

49. L.-Y. Chow Chiu Phys. Rev., 168, 32 (1968).

50. M.W.F.Shregardus thesis, University of Utrecht (1936).

51. C.Smit and H.M.Fijnaut Phys. Letters, 19, 121 (1965).

52. C.E.Kuyatt, J.A.Simpson and S.R.Mielczarek Phys. Rev., 138A, 385 (1965).

53. P.D.Burrow and J.A.Michejda, private communication.

54. M.Duweke, N.Kirchner, E.Reichert and E.Staudt J.Phys. B, 6, L208 (1973).

55. U.Fano and J.W.Cooper Phys. Rev., 138A, 400 (1965).

56. D.R.Flower and M.J.Seaton Proc. Phys. Soc., 91, 59 (1967).

Attention is drawn to the fact that the copyright of this thesis rests with its author.

This copy of the thesis has been supplied on condition that anyone who consults it is understood to recognise that its copyright rests with its author and that no quotation from the thesis and no information derived from it may be published without the author's prior written consent.